9-13-2007

Spatial Patterns of Intraseasonal Variability of Chlorophyll and Sea Surface Temperature in the California Current

K. R. Legaard

Andrew Thomas
University of Maine - Main, thomas@maine.edu

Spatial patterns of intraseasonal variability of chlorophyll and sea surface temperature in the California Current

Kasey R. Legaard[1] and Andrew C. Thomas[1]

Received 10 January 2007; revised 9 May 2007; accepted 11 June 2007; published 13 September 2007.

[1] Six years of daily satellite data are used to quantify and map intraseasonal variability of chlorophyll and sea surface temperature (SST) in the California Current. We define intraseasonal variability as temporal variation remaining after removal of interannual variability and stationary seasonal cycles. Semivariograms are used to quantify the temporal structure of residual time series. Empirical orthogonal function (EOF) analyses of semivariograms calculated across the region isolate dominant scales and corresponding spatial patterns of intraseasonal variability. The mode 1 EOFs for both chlorophyll and SST semivariograms indicate a dominant timescale of ~60 days. Spatial amplitudes and patterns of intraseasonal variance derived from mode 1 suggest dominant forcing of intraseasonal variability through distortion of large scale chlorophyll and SST gradients by mesoscale circulation. Intraseasonal SST variance is greatest off southern Baja and along southern Oregon and northern California. Chlorophyll variance is greatest over the shelf and slope, with elevated values closely confined to the Baja shelf and extending farthest from shore off California and the Pacific Northwest. Intraseasonal contributions to total SST variability are strongest near upwelling centers off southern Oregon and northern California, where seasonal contributions are weak. Intraseasonal variability accounts for the majority of total chlorophyll variance in most inshore areas save for southern Baja, where seasonal cycles dominate. Contributions of higher EOF modes to semivariogram structure indicate the degree to which intraseasonal variability is shifted to shorter timescales in certain areas. Comparisons of satellite-derived SST semivariograms to those calculated from co-located and concurrent buoy SST time series show similar features.

Citation: Legaard, K. R., and A. C. Thomas (2007), Spatial patterns of intraseasonal variability of chlorophyll and sea surface temperature in the California Current, *J. Geophys. Res.*, *112*, C09006, doi:10.1029/2007JC004097.

1. Introduction

[2] The California Current System (CCS) extends along the west coast of North America from Vancouver Island to the tip of Baja, California. Typical of major eastern boundary current systems, coastal upwelling driven by persistent equatorward wind fuels high productivity of plankton and pelagic fish. Physical and biological processes are closely coupled and vary over a wide range of time and space scales [see *Hutchings et al.*, 1995; *Smith*, 1995; *Hickey*, 1998; *Mackas et al.*, 2006]. Basin-scale oceanic and atmospheric processes alter patterns of physical forcing and biological response over interannual and decadal scales. Large-scale wind systems force latitudinally dependent seasonal cycles, including the seasonally recurrent formation of an energetic system of mesoscale jets and eddies. At smaller scales, wind-forcing and biological response fluctuate over periods of days to weeks, even at locations of seasonally sustained upwelling. Satellite remote sensing offers the sole means by which concurrent patterns of physical and biological variability can be synoptically viewed and systematically quantified across the entire region. *Legaard and Thomas* [2006] describe spatial patterns of seasonal and interannual variability across the CCS (Figure 1) using nearly six years (1997–2003) of daily sea surface temperature (SST) and chlorophyll imagery. Here we quantify dominant patterns of intraseasonal variability derived from the same data, defining intraseasonal variability as temporal variation remaining after removal of the mean seasonal cycle and interannual variability.

[3] Winds in the CCS are generally downwelling-favorable at higher latitudes (>36°N) in winter but are equatorward and upwelling-favorable along the entire coastline through late-spring and summer [*Halliwell and Allen*, 1987; *Dorman and Winant*, 1995]. The spring transition to strong and persistent equatorward winds induces a drop in coastal sea level as relatively cool, saline water is upwelled over the shelf and upper slope [*Strub et al.*, 1987; *Strub and James*, 1988]. A coastal upwelling front and surface-intensified geostrophic jet develop, reversing inshore poleward flow along the U.S. coast and reversing poleward flow or reinforcing equatorward flow along the Baja coast [*Lynn and Simpson*, 1987; *Strub et al.*, 1987; *Strub and James*, 2000]. The upwelling jet remains over the

[1]School of Marine Sciences, University of Maine, Orono, Maine, USA.

0148-0227/07/2007JC004097

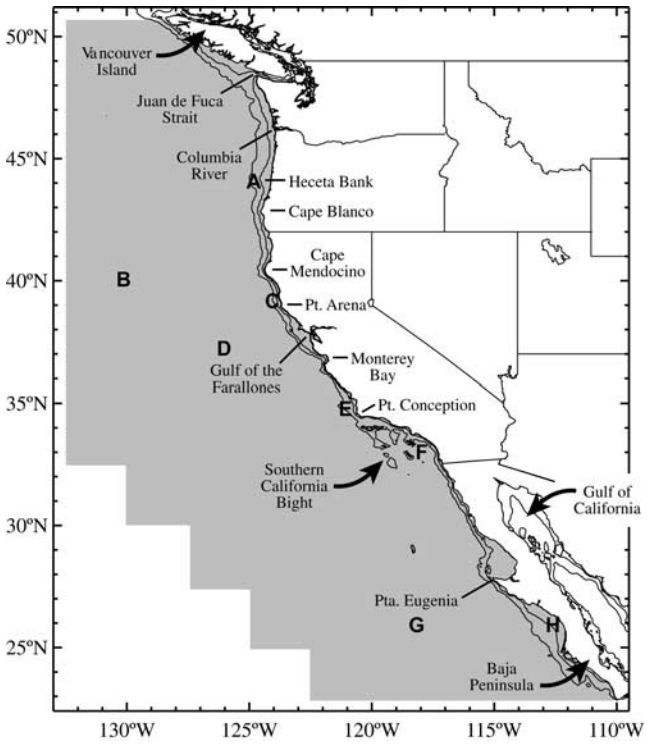

Figure 1. Map of the California Current study region, showing the area of interest (shaded) and the locations of time series data discussed within the text (a-g). Time series locations and their approximate water depths are as follows: (a) Heceta Bank, 200 m; (b) northern California offshore, >3000 m; (c) Pt. Arena, 600 m; (d) central California offshore, >3000 m; (e) Pt. Conception, 300 m; (f) eastern Southern California Bight, 600 m; (g) southern Baja offshore, >3000 m; (h) southern Baja inshore, <100 m. Locations C and E coincide with NOAA NDBC stations 46014 and 46023, respectively. Also included are 100 and 500 m isobaths.

shelf and slope of the Pacific Northwest but is quickly displaced seaward south of Cape Blanco, Oregon (42.8°N) (Figure 1) as the high-velocity core of the California Current [*Barth et al.*, 2000; *Strub and James*, 2000]. Instability processes produce meanders that develop into cyclonic and anticyclonic eddies to either side of the current core [*Marchesiello et al.*, 2003]. By late summer, equatorward winds weaken, coastal sea levels rise, and an inshore poleward countercurrent develops along south-central California and parts of Baja [*Lynn and Simpson*, 1987; *Strub and James*, 2000]. Poleward coastal currents strengthen and extend northward, displacing the upwelling jet from the shelves of the Pacific Northwest. The entire jet and eddy system migrates westward and gradually decays through the fall and winter [*Strub and James*, 2000].

[4] Multiyear time series of satellite-derived SST and chlorophyll have contributed greatly to our understanding of spatial and temporal patterns of near-surface physical and biological variability across the CCS [e.g., *Strub et al.*, 1990; *Abbott and Barksdale*, 1991; *Thomas and Strub*, 2001; *Thomas et al.*, 2001; *Legaard and Thomas*, 2006]. A typically diffuse bloom follows the spring transition to strong and sustained equatorward winds. Shortly thereafter, cool and chlorophyll-rich filaments extend from local upwelling centers from southern Oregon to the Baja Peninsula. Offshore waters become increasingly stratified and nutrient depleted. The outer boundary of productive waters develops a scalloped appearance by early to midsummer as the upwelling front and jet meander offshore of the continental margin. Chlorophyll concentrations off the coasts of California and Oregon peak at about this time, in phase with maximum equatorward winds and upwelling. Vigorous jet and eddy activity promotes the exchange of shelf and open ocean waters, and provides a local source of enrichment to offshore waters through geostrophic adjustment [*Chavez et al.*, 1991; *Strub et al.*, 1991]. Coastal surface concentrations drop in mid to late summer as winds weaken and temperatures climb toward their seasonal maxima. Following the offshore displacement of the summer circulation structure, concentrations subside to low winter levels across most of the region.

[5] Synoptic quantitative analyses of intraseasonal or mesoscale SST and chlorophyll variability have generally been limited to narrow space/time windows defined by relatively cloud-free imagery, typically of summer conditions. Off northern California, *Kelly* [1985] identifies coherent patterns of SST variability associated with local variations in wind-forcing, superimposed over a large-scale seasonal warming trend. SST imagery off central California and the Baja Peninsula demonstrate seasonally recurrent mesoscale patterns in close association with coastal topography and/or spatial variations in wind-forcing [*Lagerloef*, 1992; *Gallaudet and Simpson*, 1994; *Armstrong*, 2000]. Coastal Zone Color Scanner (CZCS) imagery off central California show rapid changes (on the order of days) of phytoplankton pigment patterns following changes in wind-forcing, superimposed over persistent and seasonally recurrent structure associated with upwelling filaments and eddies [*Abbott and Barksdale*, 1991]. Isotropic spatial power spectra calculated from CZCS images indicate that a larger proportion of total pigment variance acts over longer (shorter) wavelengths offshore (inshore), consistent with a transition from the dominance of geostrophic circulation offshore to wind-driven processes inshore [*Denman and Abbott*, 1988; *Smith et al.*, 1988]. Temporal decorrelation scales vary with spatial scale and are substantially reduced within areas just offshore of active upwelling centers [*Denman and Abbott*, 1994]. Spectral statistics of pigment and SST imagery suggest that over timescales of days to several weeks, phytoplankton behave largely as passive tracers of mesoscale circulation, with growth, death, and sinking affecting near-surface pigment distributions only minimally [*Smith et al.*, 1988; *Denman and Abbott*, 1994].

[6] Our goal is to quantify and compare physical and biological variability across the CCS (Figure 1) using concurrent time series of satellite-derived SST and chlorophyll, mapping the spatial dependence of dominant patterns of temporal variability. In a companion paper [*Legaard and Thomas*, 2006] we quantify and describe mean seasonal cycles and interannual variability. Off north-central California, seasonality is determined largely by coastal upwelling, and mean seasonal cycles of SST and chlorophyll constitute a small fraction of total variance inshore. Seasonal cycles differ at higher latitudes and in the midlatitude Southern

California Bight (SCB) (Figure 1), where upwelling winds are less vigorous and/or persistent. Strong seasonal cycles along south-central Baja appear to be driven by processes other than coastal upwelling, despite year-round upwelling-favorable winds. Patterns of interannual SST and chlorophyll variability are consistent with dominant forcing by El Niño and La Niña. Interannual SST variability is greatest along south-central Baja, but constitutes a greater fraction of total variance inshore along southern Oregon and much of California. Interannual chlorophyll variability is greatest inshore over the shelf and slope, but constitutes a greater fraction of total variance offshore. Spatial patterns of seasonal and interannual variability show considerable mesoscale structure, demonstrating seasonal recurrence of mesoscale features and suggesting that basin-scale forcing acting over interannual timescales imposes itself in many areas through changes in mesoscale pattern [*Legaard and Thomas*, 2006].

[7] Here we quantify, map, and compare dominant patterns of intraseasonal SST and chlorophyll variability. We extract intraseasonal signals from multiyear time series of daily SST and chlorophyll imagery and employ the semivariogram (or structure function) as a measure of temporal variation. Semivariograms are traditionally used to derive formal statistical models of spatial or temporal dependence suitable for optimal interpolation [e.g., *Denman and Freeland*, 1985]. Semivariograms have also been used to describe patterns of spatial and temporal variability of oceanographic data including satellite-derived SST and chlorophyll [e.g., *Denman and Freeland*, 1985; *Yoder et al.*, 1987, 2001; *Thomas and Emery*, 1988; *Fuentes et al.*, 2001; *Doney et al.*, 2003]. The semivariogram is subject to less restrictive assumptions than the covariance function or power spectrum and may provide a more stable measure of spatial or temporal dependence for many data sets. The semivariogram does not require interpolation at times or locations of missing observations and is capable of detecting and quantifying both periodic and aperiodic variation.

[8] A brief overview of the semivariogram and a detailed description of its use in this study follow in section 2. In section 3, we present dominant scales and corresponding spatial patterns of intraseasonal variation of SST and chlorophyll. In section 4, we discuss the possible origins of identified patterns, compare our results to past research, and discuss apparent limitations of our approach and of semivariogram analysis more generally. Conclusions follow in section 5.

2. Data and Methods

[9] Daily SeaWiFS Level 3 Standard Mapped Images of chlorophyll concentration from the fourth SeaWiFS reprocessing [*O'Reilly et al.*, 2000] were obtained for 4 September 1997 through 5 July 2003 from the NASA Goddard Space Flight Center Distributed Active Archive Center and subset to the CCS study area (Figure 1). These data have a nominal resolution of 9 km. Following *Campbell* [1995], we assume chlorophyll data to be approximately lognormal. To reduce the size of the data set used in subsequent calculations, chlorophyll fields were spatially averaged to geometric means within non-overlapping 18 km $\times$ 18 km boxes. Time series were assembled at each grid location from log-transformed chlorophyll concentrations. Immediately adjacent to the coastline, particularly at certain locations (e.g., the mouth of the Columbia River and the Gulf of the Farallones (Figure 1)), chlorophyll retrievals may be suspect owing to the effects of colored dissolved organic matter and light-scattering inorganic particulates. Such biases are reduced by our use of 18 km averages and are assumed to have minimal effect on our interpretation of broad-scale patterns in the CCS.

[10] Daily time series of sea surface temperature concurrent with SeaWiFS data were assembled from the NOAA/NASA AVHRR Oceans Pathfinder equal-angle, 9 km best-SST data product [*Vazquez et al.*, 1998; *Kilpatrick et al.*, 2001] provided by the NASA Physical Oceanography Distributed Active Archive Center at the Jet Propulsion Laboratory. SST estimates were derived from the Pathfinder Version 4.1 (4 September 1997 to 31 December 1999) and Interim Version 4.1 (1 January 2000 to 5 July 2003) algorithms using data from ascending passes. SST data were spatially averaged to the arithmetic mean of pixels lying within non-overlapping 18 km $\times$ 18 km boxes, and time series were assembled at each grid location.

[11] Depending on location, cloud cover and satellite orbital geometry limited the number of SST and chlorophyll observations available to $\sim$15–55% of the 2131 days within our study period. Overall patterns of data availability [*Legaard and Thomas*, 2006] reflect predominant patterns of cloud cover [*Nelson and Husby*, 1983]. Cloud cover increases and data density decreases offshore and across the northern CCS. Observations are most frequent within the SCB and along the southern Baja coast.

[12] We define intraseasonal variability as temporal variation remaining after removal of large-scale trend from each time series. Large-scale trend, or first order variation, was calculated as the sum of a regular seasonal cycle and an irregular component of interannual variation. Seasonal cycles were modeled as the sum of annual and semiannual harmonics plus a constant offset (the climatological mean). Interannual variation was estimated by smoothing non-seasonal residual time series with a 365-day Gaussian kernel. Details of these methods and descriptions of seasonal and interannual variability are presented in a companion paper [*Legaard and Thomas*, 2006]. Following the removal of mean seasonality and interannual variation, residual time series include variability acting over intraseasonal timescales, observation error, and any seasonal-scale variation not captured by stationary annual and semiannual harmonics.

[13] Figure 2 illustrates the application of our approach to time series of SST and log-transformed chlorophyll from one sample location off central Oregon (Figure 1). Trend lines (Figures 2a and 2b) represent the combined contributions of seasonal and interannual variation, accounting for 81% and 36% of the total temporal variance of SST and chlorophyll, respectively. Residual time series of SST and chlorophyll (Figures 2c and 2d) display considerable year-to-year variation. Note for example that large-scale trend overestimates temperatures during the transition from El Niño to La Niña conditions in early 1999. Such indications of nonstationarity over long timescales motivate our use of the semivariogram as a quantitative descriptor of intraseasonal variation.

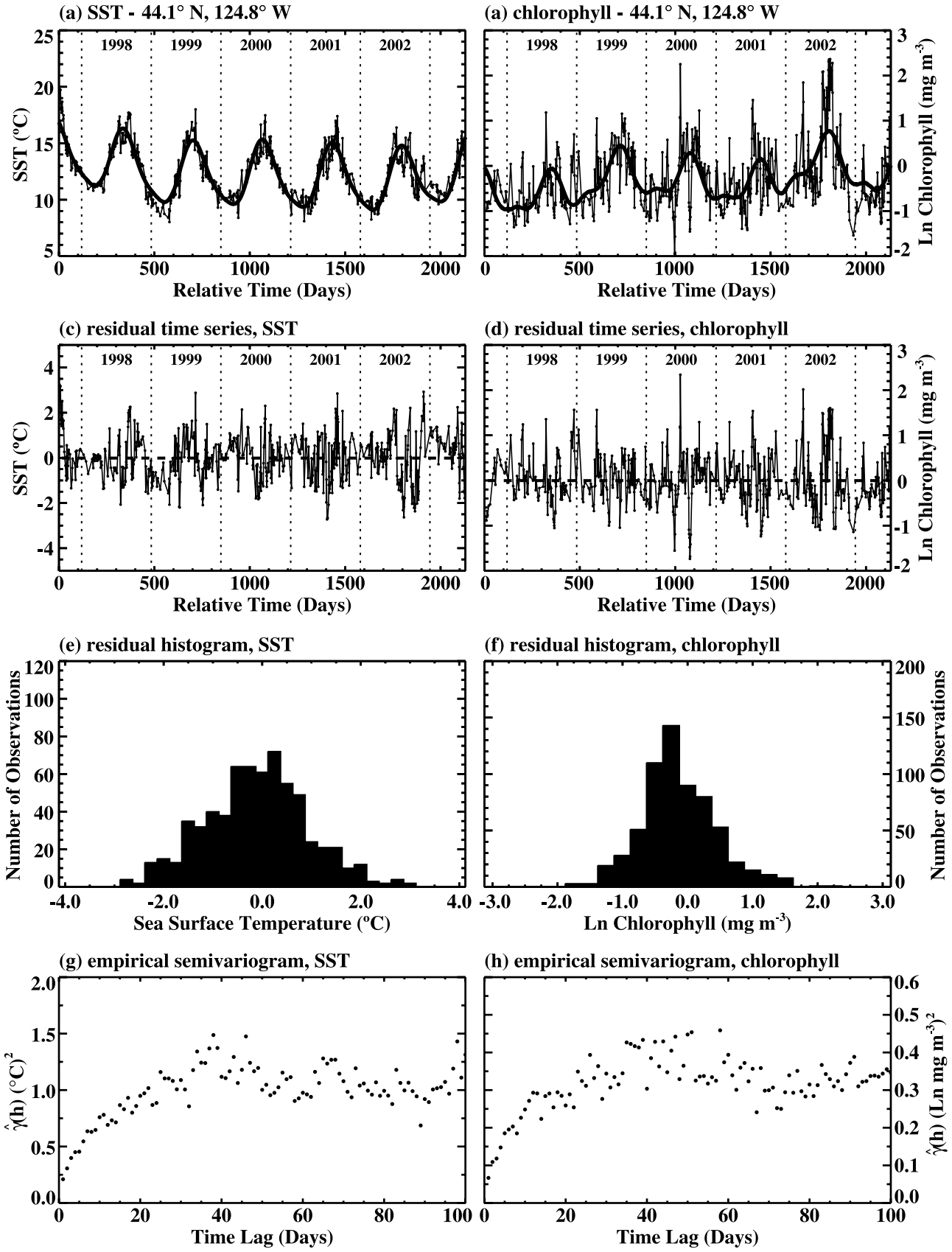
(a) SST - 44.1° N, 124.8° W
(a) chlorophyll - 44.1° N, 124.8° W
1998
1999
2000
2001
2002
SST (ºC)
Ln Chlorophyll (mg m-3)
Relative Time (Days)
(c) residual time series, SST
(d) residual time series, chlorophyll
(e) residual histogram, SST
(f) residual histogram, chlorophyll
Number of Observations
Sea Surface Temperature (ºC)
Ln Chlorophyll (mg m-3)
(g) empirical semivariogram, SST
(h) empirical semivariogram, chlorophyll
γ̂(h) (°C)2
γ̂(h) (Ln mg m-3)2
Time Lag (Days)

Figure 2

[14] A thorough review of the semivariogram and its properties may be found in any number of geostatistics texts [e.g., *Goovaerts*, 1997; *Webster and Oliver*, 2001]. Here we present a brief overview. Consider a residual time series $Z(t)$ as a random function composed of a set of random variables $Z(t_i)$ corresponding to the N observations available at that location. The covariance C between any two random variables $Z(t_i)$ and $Z(t_j)$ constitutes a measure of the similarity between the two and is defined as

$$C\big(Z(t_i), Z\big(t_j\big)\big) = E\big\{[Z(t_i) - \mu(t_i)] \cdot \big[Z\big(t_j\big) - \mu\big(t_j\big)\big]\big\} \quad (1)$$

where $\mu(t_i)$ and $\mu(t_j)$ are the means of $Z(t_i)$ and $Z(t_j)$, and where $E(\cdot)$ is the expectation function. Use of the covariance function as a measure of temporal dependence for the time series $Z(t)$ requires the assumption of a constant mean for all $Z(t_i)$ and a finite covariance that depends only on the time lag $h = t_j - t_i$. These assumptions constitute second order or weak stationarity and imply the absence of any first order variation of the mean. Where annual and semiannual harmonics fail to capture year-to-year changes in the timing or magnitude of the seasonal cycle, significant seasonal-scale variability may remain, and residual time series may display modest departures from weak stationarity. If however the local mean of the residual series remains constant over short time lags, we can assume that

$$E[Z(t) - Z(t+h)] = 0 \quad (2)$$

for small h. If we assume weak stationarity of the increments $[Z(t_i) - Z(t_j)]$ rather than the random variables themselves, the variance of the difference $[Z(t) - Z(t+h)]$ can be used as an alternative measure of temporal dependence:

$$\gamma(h) = \frac{1}{2}\mathrm{var}[Z(t) - Z(t+h)] \quad (3)$$

The quantity $\gamma(h)$ for a given time lag h is referred to as semivariance and constitutes a measure of the average dissimilarity between data values separated by the lag h. The function $\gamma(h)$ is the semivariogram. Equations (2) and (3) constitute intrinsic stationarity, a form of stationarity in which only local homogeneity is assumed. The semivariogram $\gamma(h)$ provides a valid description of spatial or temporal dependence in many cases where departures from weak stationarity follow from the incomplete removal of large-scale trend. This wider range of validity makes the semivariogram more useful than the covariance function for a variety of applications.

[15] For an autocorrelated and weakly stationary time series, the semivariogram is a mirror image of the covariance function. The semivariogram climbs from small values at shorter lags to large values at longer lags, attaining or asymptotically approaching an upper bound referred to as the sill, equal to the overall variance of the process. The range is defined as the lag at which semivariance attains (or closely approaches) the sill. Covariance drops to zero at the range so that observations separated by greater lag times are no longer correlated. Regular repetition or periodicity causes a peak in semivariance at a time lag equal to one-half of the dominant period. Peak semivariance corresponds to negative correlation between data pairs, and generally exceeds the overall variance. Multiple scales of variability may lead to multiple, irregularly spaced peaks or sills. The time lag of a prominent peak corresponds to a dominant scale of variability and the value of peak semivariance corresponds to the magnitude of variability (mean data dissimilarity) acting at that scale.

[16] Histograms compiled from residual time series at our sample location (Figures 2e and 2f) show that although SST residuals are near-normal, chlorophyll residuals are somewhat skewed. Chlorophyll residuals are moderately skewed at nearly all locations and residual distributions of both variables typically display thicker tails than expected for a normal process. We therefore employ an estimator of empirical semivariance derived by *Cressie and Hawkins* [1980] for similar distributions:

$$\hat{\gamma}(h) = \frac{\frac{1}{2}\left(\frac{1}{n(h)}\sum_{n(h)}|Z(t_i) - Z(t_i+h)|^{\frac{1}{2}}\right)^4}{\left(0.457 + \frac{0.494}{n(h)}\right)} \quad (4)$$

where $n(h)$ is the number of pairs of observations separated by the time lag h. Semivariance was estimated to a maximum time lag of 100 days, below which most (of the residual) temporal structure of interest occurred. The analytical derivation of confidence limits for estimates of semivariance is complicated by nonrandom sampling of the underlying process, correlations between estimates, and use of the same data in multiple estimates [*Webster and Oliver*, 2001]. For practical applications, the assessment of what constitutes a statistically sufficient number of data pairs to estimate semivariance at a given lag is somewhat subjective. We considered an estimate of semivariance to be valid if at least 30 data pairs were used in its calculation, a criterion previously employed for the estimation of spatial semivariograms from SeaWiFS data [*Fuentes et al.*, 2001; *Doney et al.*, 2003]. Only valid estimates were included in subsequent analyses.

[17] Empirical estimates of semivariance are subject to error arising primarily from incomplete sampling of the underlying process. Here, intermittent cloud cover contributed scatter to all semivariograms. Nevertheless, SST and chlorophyll semivariograms calculated at our sample location (Figures 2g and 2h) show clear trends suggesting peak

Figure 2. Time series of (a) Pathfinder SST and (b) SeaWiFS chlorophyll assembled at 44.1°N, 124.8°W (location shown in Figure 1). Thick solid lines represent large-scale trends composed of seasonal cycles and an irregular component of interannual variation. Residual time series of (c) SST and (d) chlorophyll calculated by subtracting large-scale trend from the original time series. Histograms of (e) SST and (f) chlorophyll residual time series. Empirical semivariograms estimated from (g) SST and (h) chlorophyll residual time series.

values at ~40–50 days, corresponding to dominant periods of ~80–100 days. As lag time decreases toward zero, empirical estimates of semivariance typically appear to approach a positive value referred to as nugget semivariance. The nugget arises from measurement error and unresolved variation acting over timescales shorter than the sampling interval. Both sample semivariograms indicate a nugget effect. Residual time series are therefore composed of a temporally correlated component of variability superimposed over an uncorrelated, random component whose contribution is given by the nugget. At this sample location, nugget values lie within the accepted error variance of the SST (http://podaac.jpl.nasa.gov/sst/) and chlorophyll data [*O'Reilly et al.*, 2000], suggesting that instrument and algorithm error are a major component of the nugget.

[18] In order to objectively discriminate coherent structural features from empirical semivariograms, an Empirical Orthogonal Function (EOF) analysis was performed on the SST and chlorophyll semivariance data sets. Prior to analysis, empirical semivariograms were centered and normalized so that EOF modes were not biased by semivariograms computed from high-variance time series. EOF analysis decomposed the spatially distributed sets of semivariograms into a set of orthogonal functions describing characteristic patterns of semivariance and a set of spatial amplitude functions describing the relative contribution of each EOF to the (normalized) empirical semivariogram calculated at each grid location. Each EOF mode was assumed statistically significant provided it explained a greater amount of structure than did 95% of the corresponding modes derived from analyses of 100 random data sets of the same size [*Overland and Priesendorfer*, 1982]. The mode 1 EOF describes the semivariogram shape most representative of empirical semivariograms calculated throughout the region. The combined structure assigned to significant higher modes describes coherent structural deviations from the mode 1 semivariogram. We present all spatial amplitude maps after smoothing with a 5 × 5 moving average to reduce speckling and emphasize large-scale patterns of interest.

3. Results

3.1. Empirical Semivariograms

[19] Eight grid locations (Figure 1) were selected to illustrate empirical semivariograms. Locations were chosen to reflect the range of seasonal, interannual, and intraseasonal behavior evident in the regional SST and chlorophyll data. Empirical semivariograms calculated from residual time series at these locations (Figure 3) show that despite considerable scatter, consistent structural variations are apparent between locations. At inshore locations off Oregon and California (Figures 3a, 3c, and 3e), semivariance increases sharply over the first ~10–20 days, attaining maximum or near-maximum values by ~20–40 days. At offshore locations (Figures 3b, 3d, and 3g), semivariograms show a more gradual increase to an apparent sill at ~40–60 days. A rapid rise over short lags at nearshore locations indicates a rapid loss of correlation with increasing separation time, consistent with a large amount of variation acting over short timescales. In contrast, a more gradual rise to maximum semivariance at longer lags indicates greater temporal continuity offshore. Also note that small sills and large nuggets (relative to the size of the sill) indicate lower levels of resolved intraseasonal variation offshore. Scatter between empirical estimates of semivariance is least pronounced and semivariogram structure most clearly defined at inshore locations where data density is the greatest [*Legaard and Thomas*, 2006], most notably off southern California and the Baja coast (e.g., Figures 3f and 3h). Semivariogram structure is more poorly defined far from shore (e.g., Figure 3g) where SST and chlorophyll variability is weak and data density reduced. The shapes of chlorophyll and SST semivariograms are very similar at some locations (e.g., off central Oregon, Figure 3a) and very dissimilar at others (e.g., off southern California, Figure 3e).

3.2. Dominant Semivariogram Structure and Spatial Patterns

[20] EOF analyses summarize dominant structure of SST and chlorophyll semivariograms across the study region. Mode 1 explains 62% and 48% of SST and chlorophyll semivariance structure. Mode 2 explains 4% of the semivariance structure of both variables. Modes 3 and 4 are marginally significant, collectively explaining 3% and 4% of SST and chlorophyll semivariance structure. Structure not explained by the first four modes (31% and 44% for SST and chlorophyll) is distributed more or less evenly across the remaining insignificant modes, reflecting the considerable scatter within individual semivariograms (Figure 3).

[21] Dominant shapes of both SST and chlorophyll semivariograms (mode 1 EOFs, Figures 4a and 4b) follow an inverse negative exponential curve approaching an asymptotic upper bound at 50–60 days. The chlorophyll mode 1 function increases smoothly; the SST function displays a well-defined 8–10 day oscillation superimposed over the general curve. Similar though less coherent oscillations are often apparent in empirical SST semivariograms (Figure 3) and appear to reflect a tendency for observations to be systematically grouped at this sampling interval. *Walker and Wilkin* [1998] describe a similar tendency in Pathfinder SST data over the Indo-Australian region and suggest satellite orbital characteristics as its cause. We discuss the sampling structure of SST time series further in section 4.3. We do not identify a specific decorrelation scale from the mode 1 EOF. While EOF analysis defines dominant semivariogram structure common to large areas, locally important structure can be relegated to statistically insignificant higher modes. Location-specific decorrelation scales are sensitive to small changes in semivariogram shape and are generally more spatially variable than the patterns revealed by EOF analysis. We attempted various means of defining decorrelation scales or dominant scales of variability from individual semivariograms [e.g., *Yoder et al.*, 1987, 2001; *Fuentes et al.*, 2001] but found no approach that provided a consistent and reliable means of delineating regional patterns of variability.

[22] Spatial amplitude functions (Figures 4c and 4d) describe the relative contributions of the mode 1 semivariograms at each grid location. Small values reflect either a structural dissimilarity between the mode 1 EOF and local semivariogram shape or increased scatter between empirical semivariance estimates. SST amplitudes (Figure 4c) are greatest within several hundred kilometers of the Baja

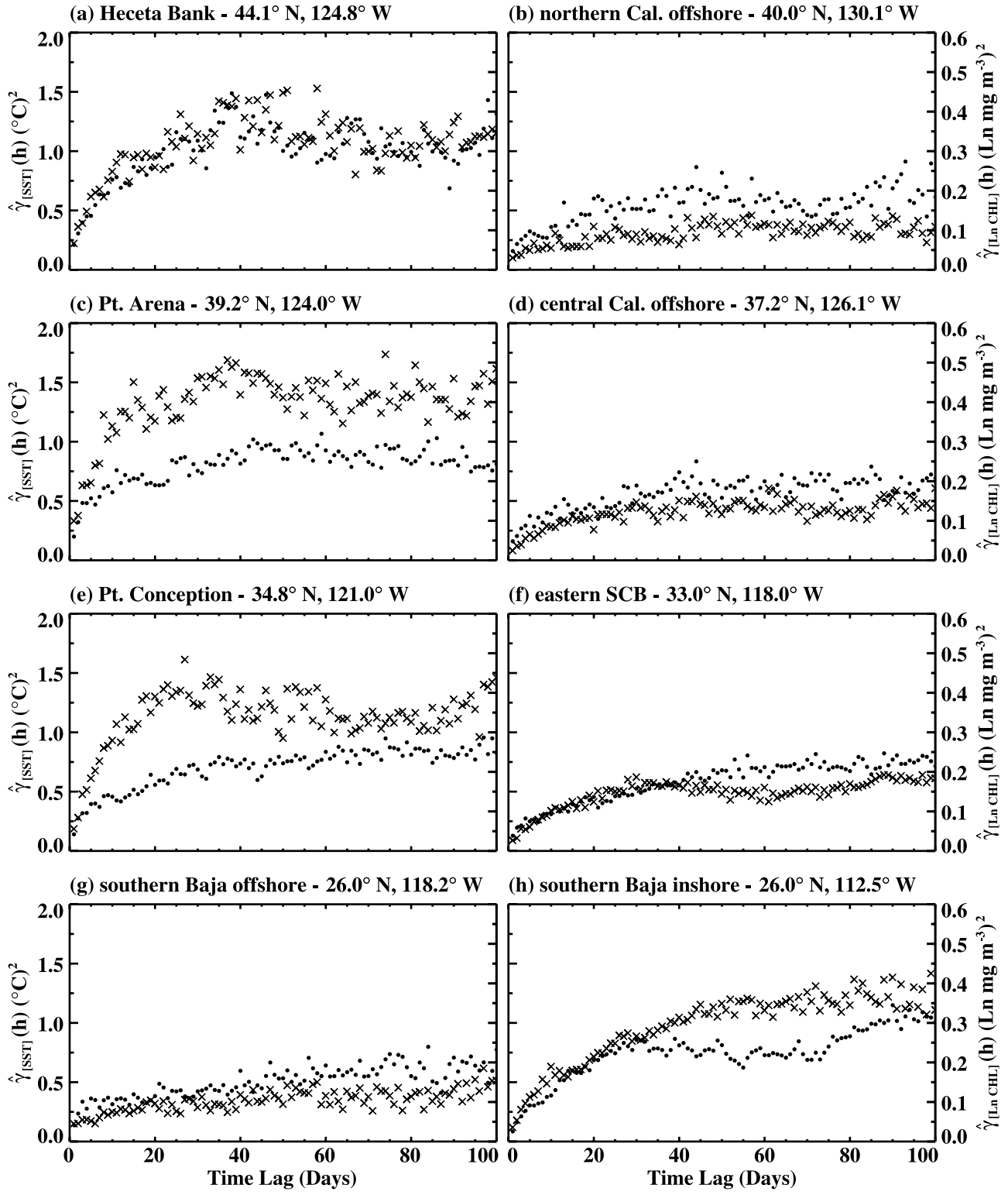

Figure 3. (a-h) Empirical semivariograms calculated from residual time series of Pathfinder SST (•) and SeaWiFS chlorophyll (×) assembled at the eight locations shown in Figure 1. SST and chlorophyll axes are plotted to the left and right, respectively.

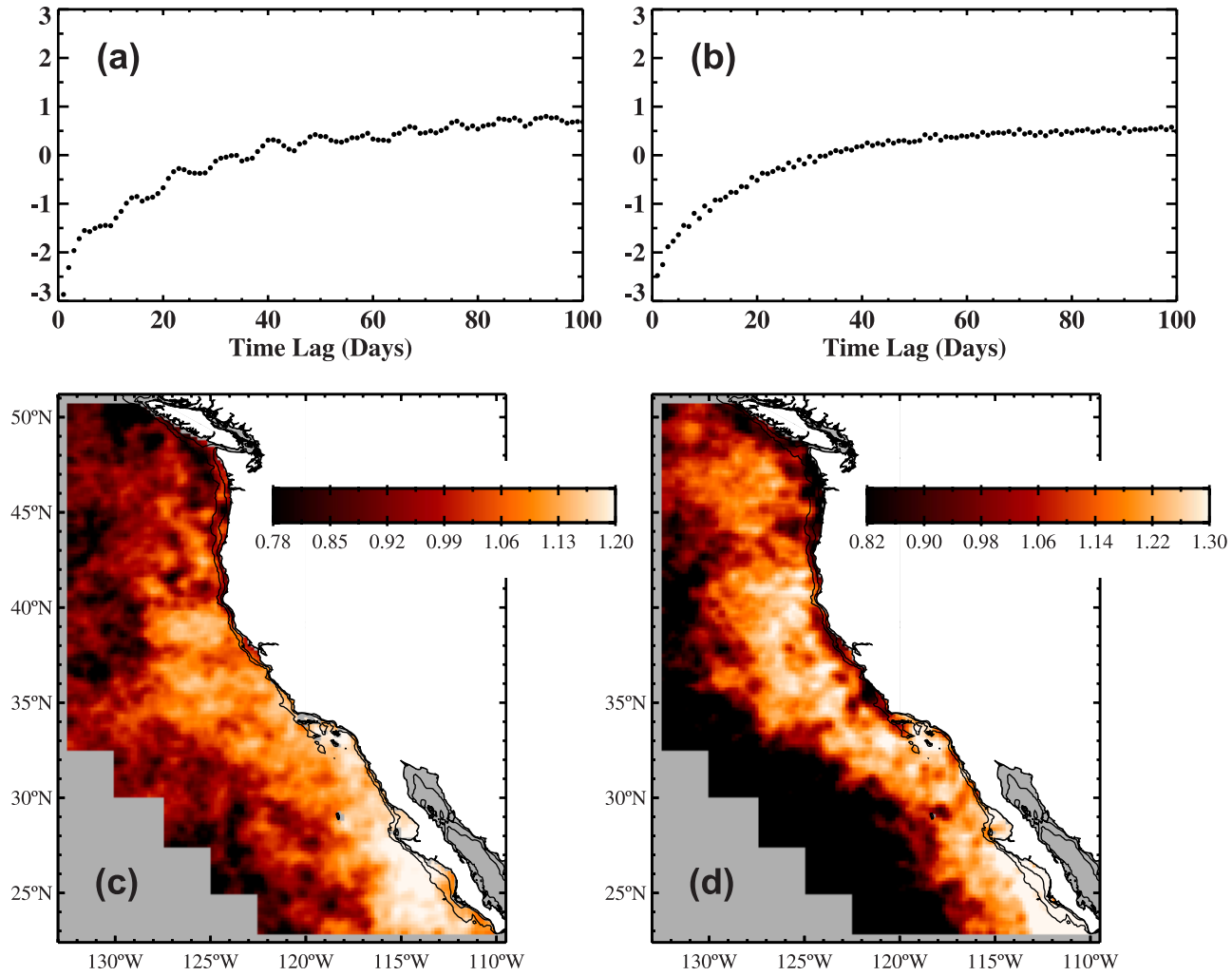

Figure 4. Mode 1 EOF for semivariograms calculated from (a) Pathfinder SST and (b) SeaWiFS chlorophyll. Mode 1 spatial amplitude functions for semivariograms calculated from (c) SST and (d) chlorophyll.

Peninsula and Southern California. Nearshore amplitudes gradually decrease to the north but remain broadly elevated (>1.0) within a band extending ~400–500 km offshore, from the southern limit of our study region to ~40°N. North of Cape Mendocino (40.4°N) (Figure 1), the width of this band tapers toward the coastline of central Oregon. SST semivariograms at locations north of ~45°N or more than ~500 km offshore are generally poorly represented by mode 1, compared to semivariograms at more southerly and inshore locations. As with SST, chlorophyll amplitudes (Figure 4d) are elevated within 400–500 km of the coastline south of northern California (~42°N), with maximum values off southern Baja. Elevated amplitudes also extend into the northern portion of our study region where mode 1 SST amplitudes are relatively low. Maximum chlorophyll amplitudes are separated from the coast by a narrow band (~100 km) of low amplitude extending from Vancouver Island south to Point Conception (34.4°N) (Figure 1), widest north of Cape Blanco (~43°N) and off south-central California (centered at ~35°N).

[23] Mode 2 EOFs and spatial amplitude functions describe the most coherent deviation from the dominant structure defined by mode 1. For SST (Figure 5a), the mode 2 EOF reduces semivariance at short lags (<10 days) and long lags (>60 days) and increases semivariance over a broad interval centered at ~40 days. The space pattern (Figure 5c) shows an irregular band of positive amplitude within ~200 km of the Pacific Northwest, extending southwestward from southern Oregon and northern California to the outer boundary of the study region. Relative to the structure defined by mode 1, SST semivariograms in this band tend to show a sharper rise over shorter lags and a shift in peak semivariance to ~40 days, often followed by a modest drop at longer lags (e.g., Figure 3a). The weak negative amplitudes found elsewhere in the study region define a slight increase in semivariance at shorter and longer lags and a decrease at intermediate lags. Stronger negative values offshore of Baja indicate a greater flattening of the mode 1 pattern (e.g., Figure 3g). The weak negative mode 2 contributions and modes 3 and 4 (not shown) do not bear a substantial or widespread influence on dominant semivariogram structure. The mode 2 chlorophyll EOF (Figure 5b) is similar to that of SST, negative at short lags and gradually increasing to a broad peak centered at ~40 days. Strong positive amplitudes (Figure 5d) are concentrated within 100–200 km of the coast off north-central California

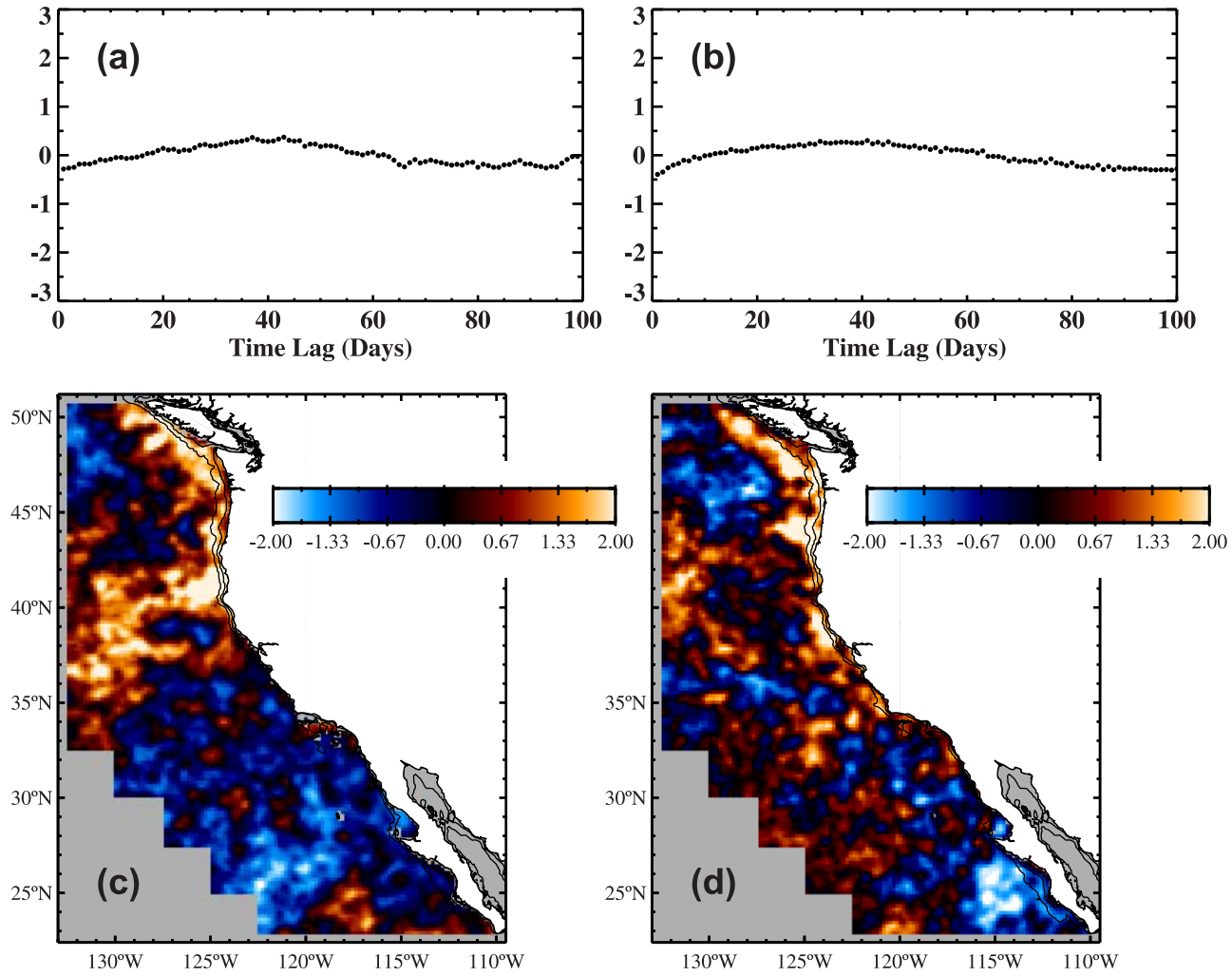

Figure 5. Mode 2 EOF for semivariograms calculated from (a) Pathfinder SST and (b) SeaWiFS chlorophyll. For comparison with mode 1 EOFs, y-axes retain the scaling of Figure 4. Mode 2 spatial amplitude functions for semivariograms calculated from (c) SST and (d) chlorophyll. To highlight spatial patterns, data scaling differs from the mode 1 spatial amplitude functions of Figure 4.

(centered at ~39°N), north of Cape Blanco (~43°N), and immediately seaward of the shelf off Vancouver Island, indicating a sharper rise over short lags (e.g., Figures 3a and 3c). Strong negative amplitudes off southern Baja indicate a weaker initial rise and flattening of the mode 1 structure. Modes 3 and 4 (not shown) are strongest in a localized area within ~100 km of the California coast south of Monterey Bay (~37°N) (Figure 1), shifting peak semivariance to ~25–30 days (e.g., Figures 3e and 3f). Contributions of modes 3 and 4 are much less spatially extensive than that of mode 2.

3.3. Variance Estimation

[24] Variance attributable to dominant intraseasonal structure and coherent deviations from dominant structure is quantified and compared by reconstructing semivariograms from mode 1 and modes 2–4, respectively (Figure 6). The product of the mode 1 EOF and spatial amplitude estimate provides a reasonable approximation to the original empirical semivariogram calculated at most locations, once rescaled and recombined with the mean of the original. The mode 1 reconstruction of semivariance is approximated by an exponential model:

$$\gamma(h) = \begin{bmatrix} 0 & h = 0 \\ c_0 + (\sigma^2 - c_0)\left(1 - e^{-3h/r}\right) & h \neq 0 \end{bmatrix} \quad (5)$$

where c_0, σ^2, and r are the nugget, sill, and range parameters, respectively. Where the mode 1 EOF is fully representative of semivariogram shape (i.e., where the contributions of modes 2–4 are weak), sill and nugget parameters estimate the overall variance and unresolved variance of the residual time series. The range is implicitly defined as the lag at which semivariance has increased to 95% of the asymptotic sill. Nugget, range and sill parameter estimates were obtained at each grid location through a nonlinear least squares fit of the exponential model to each mode 1 reconstruction. Range estimates for SST (chlorophyll) were typically about 65 days (56 days), equivalent to an e-folding scale of 22 days (19 days). Because model

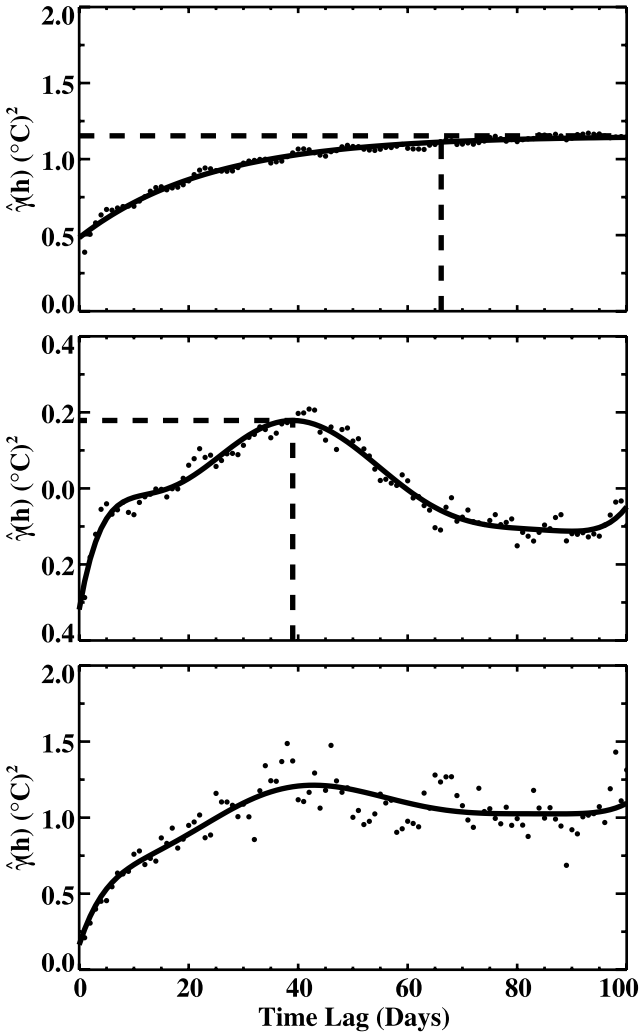

Figure 6. Reconstruction of semivariance estimated from Pathfinder SST data collected at 44.1°N, 124.8°W (location shown in Figure 1). (a) Mode 1 reconstruction. The thick solid line is the exponential curve fit to the mode 1 structure. Vertical and horizontal dashed lines are the mode 1 range and sill estimates, respectively. (b) Modes 2–4 reconstruction. The thick solid line is the polynomial curve fit to the modes 2–4 structure. Vertical and horizontal dashed lines identify the timescale and magnitude of the peak contribution of modes 2–4. Note the change of scale for the y axis. (c) Empirical semivariogram. The thick solid line is the sum of the mode 1 exponential curve and the modes 2–4 polynomial curve.

fits were applied to a single semivariance structure common to all locations, range estimates varied little.

[25] The contribution of statistically significant higher modes was calculated as a weighted sum of the second, third, and fourth EOFs, with weights provided by the corresponding spatial amplitude functions. To capture their more variable structural contributions, reconstructions of semivariance based on modes 2–4 were modeled by eighth-order polynomials (Figure 6b). The combined contributions of the mode 1 exponential and the high-mode polynomial model generally provide a satisfactory representation of the form of the original empirical semivariogram (Figure 6c). The magnitude of the most prominent peak of the high-mode polynomial provides a measure of variance introduced by modes 2–4 at the scale defined by the peak's location. Peak high-mode semivariance is superimposed over the dominant contribution of mode 1, and therefore indicates the degree to which temporal structure is shifted toward shorter timescales at each grid location. An improved estimate of nugget variance is provided by the sum of the mode 1 nugget parameter and y-intercept of the high-mode polynomial. Because chlorophyll semivariograms were calculated from log-transformed data, estimates of the mode 1 sill, peak high-mode semivariance, and nugget were rescaled into the original data units in a manner analogous to that described by *Fuentes et al.* [2001] for spatial semivariograms. Maps are presented after smoothing with a 5 × 5 moving average to reduce speckling.

3.4. Spatial Patterns of Unresolved Geophysical Variance, Error, and Noise

[26] The geographic distribution of unresolved SST variance (nugget estimates, Figure 7a) shows elevated values (>0.20°C^2) centered just off the Pacific Northwest shelf (north of ~45°N) and adjacent to the coast between Cape Mendocino and Point Conception. Very low values (<0.05°C^2) lie along the coast within the eastern SCB and just south of Cape Blanco and Punta Eugenia (27.7°N) (Figure 1). Because empirical semivariograms show the least scatter inshore where data density is greatest, nugget estimates in coastal areas may have a strong contribution from unresolved geophysical variation. Far offshore where data density is least, elevated nugget values are consistent with strong contributions from estimation error and noise. Nugget estimates are affected by model fit at short lags and nugget estimates provided here may be affected by variations in the partitioning of short time-scale structure between EOF modes. However, mean SST nugget variance over the entire study area is 0.14°C^2, very similar to the unresolved variance of 0.15°C^2 for Pathfinder SST time series reported by *Walker and Wilkin* [1998] for the Indo-Australian region, using empirical estimates of covariance. A nugget variance of 0.14°C^2 corresponds to an estimation error of 0.37°C, well within the accepted error of 0.3–0.5°C for Pathfinder data (http://podaac.jpl.nasa.gov/sst/).

[27] The spatial pattern of unresolved chlorophyll variance (nugget estimates, Figure 7b) is similar to annual mean concentrations [*Legaard and Thomas*, 2006], high over most shelves and low offshore. Estimates are highest over the broad shelves of the Pacific Northwest and within the Gulf of the Farallones. Coastal nugget estimates and mean concentrations are both lowest within the SCB and along the northernmost Baja coast. These patterns are consistent with those reported by *Doney et al.* [2003] for global patterns of satellite-measured chlorophyll spatial structure, where nugget variance resulted from measurement error and submesoscale spatial structure with dimensions on the order of 10 km, and varied in proportion to mean concentrations where they exceeded ~0.2 mg m^{-3}. At lower concentrations (our offshore regions), nugget estimates reflect a low level of background variation attributed to instrument and algorithm error. Throughout the CCS, nugget values generally

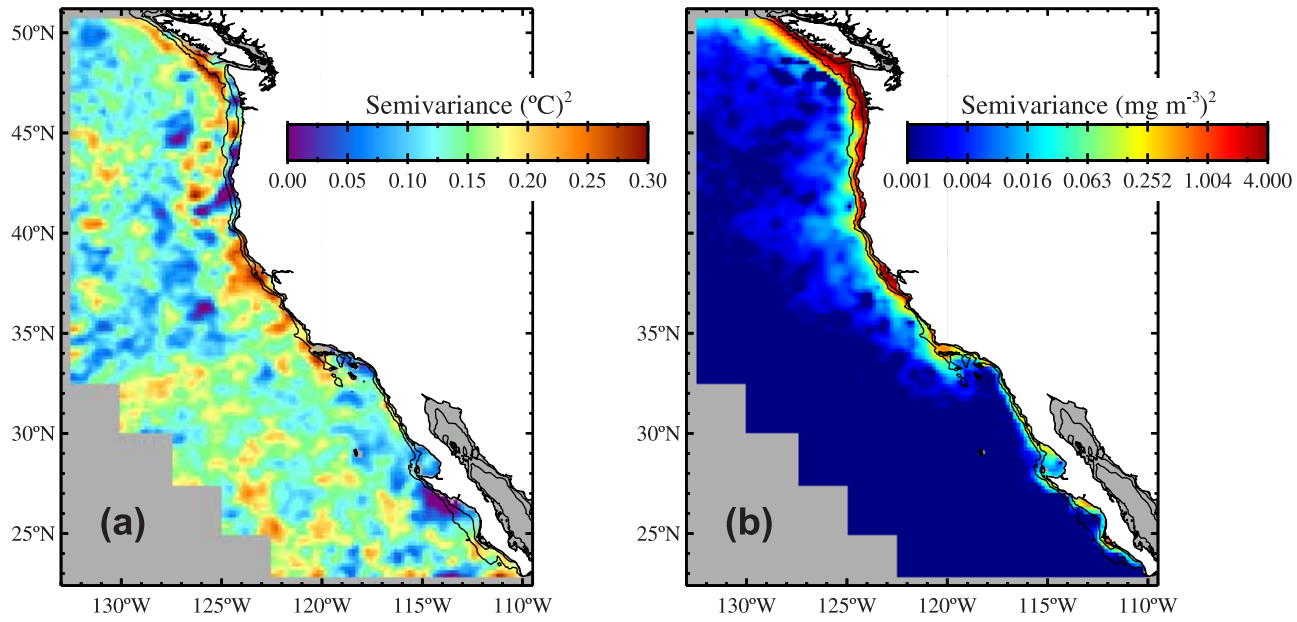

Figure 7. Unresolved variance of (a) Pathfinder SST and (b) SeaWiFS chlorophyll, calculated as the combined contribution of the nugget parameter estimate of the mode 1 exponential model and the y-intercept of the modes 2–4 polynomial model.

lie within the accepted error variance of the satellite-derived chlorophyll estimates [*O'Reilly et al.*, 2000].

3.5. Spatial Patterns of Intraseasonal Variance

[28] Spatial patterns of the magnitude of intraseasonal variance of SST (mode 1 sill estimates, Figure 8a) show high values (>1.0°C^2) generally confined to two areas; the first extends ~200 km offshore of southern Oregon and northern California and the second extends seaward of southern Baja to ~116°W. Lowest values occupy offshore areas, intruding closest to the coast in the SCB and along northern Baja. As a fraction of total SST variance (Figure 8c), the strongest contributions of dominant intraseasonal variability (exceeding 40% of total variability) lie near upwelling centers at Cape Blanco and Cape Mendocino. Intraseasonal contributions are elevated within ~200 km of shore from southern Oregon to Point Conception, accounting for about 25% of total SST variability. Within these areas, seasonal contributions are relatively low (accounting for less than ~60% of total variability), and intraseasonal and interannual contributions are relatively high [*Legaard and Thomas*, 2006]. Where seasonal contributions to total variance are comparatively greater along the Baja Peninsula, within the SCB, along the Pacific Northwest shelf, and everywhere offshore, intraseasonal contributions are lower (<20%) (Figure 8c).

[29] Chlorophyll intraseasonal variance estimates (mode 1 sill estimates, Figure 8b) follow a spatial distribution similar to mean chlorophyll concentrations and, where elevated near the shelf and slope, similar to annual and semiannual amplitudes [*Legaard and Thomas*, 2006]. Maximum sill estimates lie over the Pacific Northwest shelf (north of Cape Blanco) and within the Gulf of the Farallones. The highest values (>1.0 (mg m^{-3})^2) extend farthest from shore off Washington and Vancouver Island and are confined close to shore along Baja. Elevated values (>0.1 (mg m^{-3})^2) extend offshore of northern and central California and along the outer boundary of the SCB, but are closely confined to the Baja shelf. Sill estimates are low everywhere offshore, especially in the southern portion of the study region. Nearshore, they are relatively low over the deep basins of the eastern SCB and along the Baja coast.

[30] As a fraction of total chlorophyll variance, the magnitude of dominant intraseasonal variability (Figure 8d) reflects many of the same features evident in patterns of seasonality, with areas of strong intraseasonal contributions coincident with areas of weak seasonal contributions [*Legaard and Thomas*, 2006]. Interannual contributions are generally very low (<10%) except within relatively discrete mesoscale features offshore of California and within a broad area offshore of Baja [*Legaard and Thomas*, 2006]. In offshore areas between ~35°N and ~43°N, extending inshore (east) to a scalloped boundary off California, strong annual cycles dominate chlorophyll variability and intraseasonal contributions are correspondingly low (<30%). This is the eastern end of the North Pacific transition zone, a latitudinal band where summer stratification alternates with deep winter mixing and an annual "standing wave" of production migrates meridionally with the depth of the seasonal mixed layer [*Lewis et al.*, 1988]. Within the subtropical gyre to the south where seasonality is very weak, intraseasonal contributions are very high (>90%). Intraseasonal variation within subtropical waters is, however, poorly resolved by daily time series [*Uz and Yoder*, 2004], and sill estimates in this area reflect large nugget contributions (e.g., Figure 3g). Dominant intraseasonal variation accounts for more than 70% of total variability in most inshore areas save for the southern Baja shelf where seasonal cycles dominate. The greatest nearshore intraseasonal contributions lie along southern Oregon and north-central California, inshore of weak contributions within the North Pacific transition

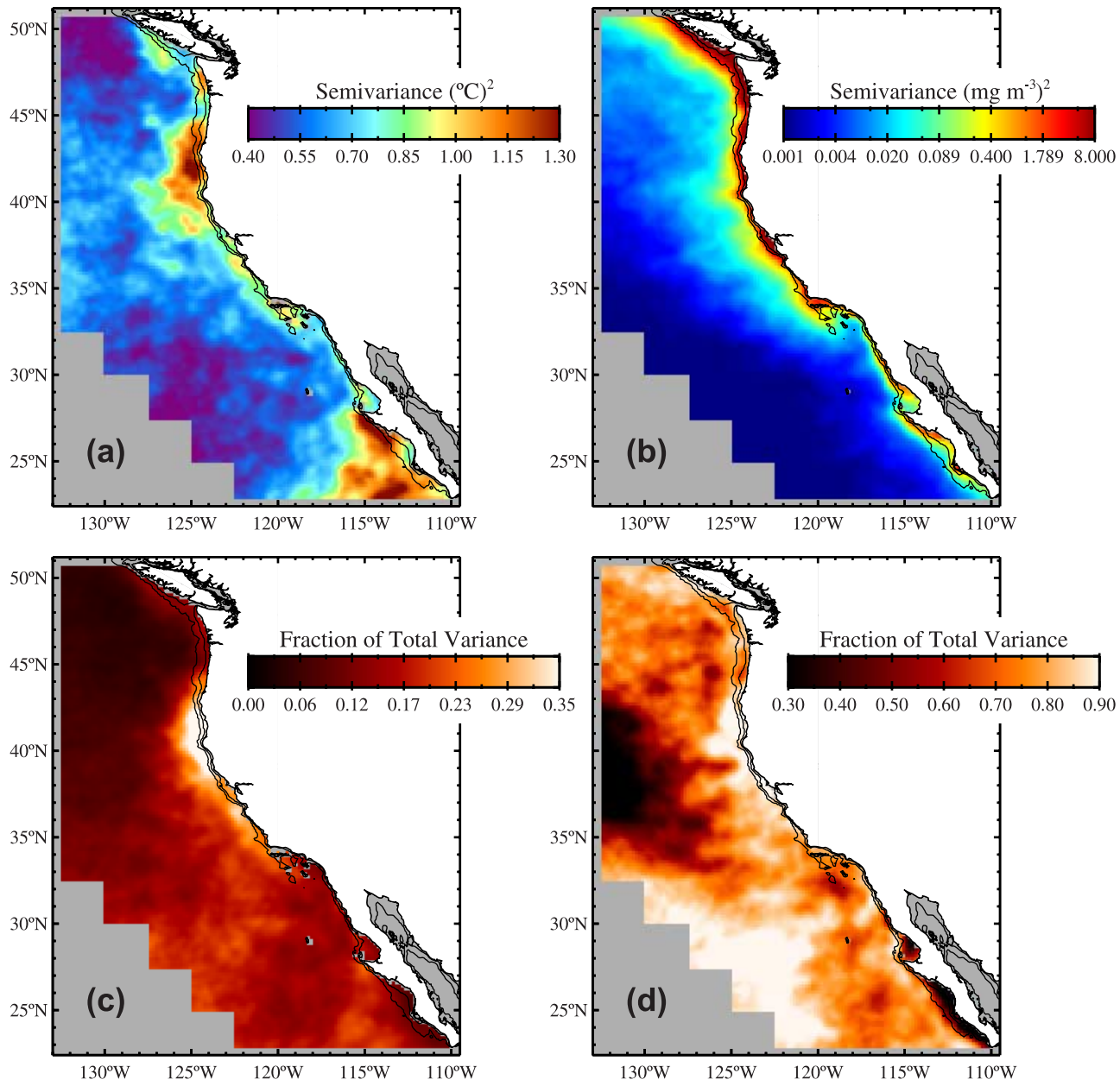

Figure 8. Variance attributable to the dominant intraseasonal structure of (a) Pathfinder SST and (b) SeaWiFS chlorophyll, calculated as the sill of the exponential model fit to mode 1 semivariograms. Fraction of total variance attributable to the dominant intraseasonal structure of (c) SST and (d) chlorophyll. Total variance is approximated as the sum of variance contributed by dominant intraseasonal variability and the mean seasonal cycle and interannual variability described by *Legaard and Thomas* [2006].

zone. The scalloped boundary between these two areas coincides with the early summer path of the California Current core as it extends offshore of Cape Mendocino and Point Arena (39.2°N) (Figure 1) in well-defined meanders [*Strub et al.*, 1991; *Strub and James*, 2000].

[31] The magnitude of peak semivariance for modes 2–4 provides a relative measure of the combined influence of these higher modes, which we interpret as the degree to which temporal variation is shifted to scales shorter than that of the dominant mode 1 structure. Spatial patterns for SST (Figure 9a) show the greatest high-mode contributions (>0.15°C^2) along southern Oregon and northern California, extending ~200 km offshore between Cape Blanco and Cape Mendocino. Weaker and more diffuse bands of elevated semivariance extend along the coast to the north and offshore to the southwest, similar in pattern to that of the strong positive mode 2 amplitudes (Figure 5c). Peak high-mode semivariance values exceeding 0.08°C^2 (Figure 9a) occur at an average time lag of 39 days, confirming the dominance of mode 2 in defining structural deviations from the mode 1 EOF. Statistically significant higher modes introduce very little structure throughout the remainder of

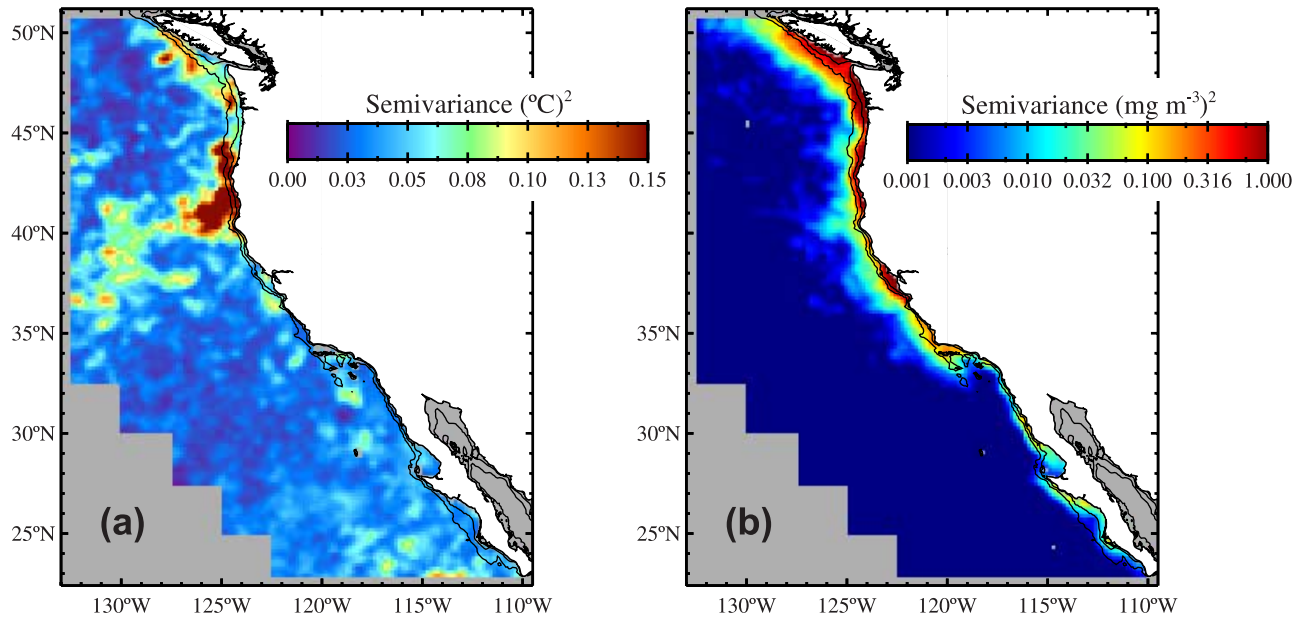

Figure 9. Variance attributable to coherent deviations from dominant intraseasonal structure for (a) Pathfinder SST and (b) SeaWiFS chlorophyll, estimated as the magnitude of peak semivariance introduced by modes 2–4.

the region. While more localized variations in SST semivariogram shape do occur (e.g., Figure 3h), EOF decomposition isolates the most coherent structure occurring over large areas.

[32] The spatial distribution of peak high-mode semivariance for chlorophyll (Figure 9b) is similar to that of mode 1 (Figure 8b), though much less in all areas and with reduced offshore extension. Maximum values are centered over lags of ~20–45 days close to the coast where modes 2–4 play a prominent role in describing semivariogram shape. The time lags of peak high-mode semivariance (at high-variance locations) are considerably more variable than those of SST, consistent with the stronger contributions of the less coherent, more locally variable modes 3 and 4. Close to shore from Vancouver Island to Point Conception and along the outer boundary of the SCB, where mode 1 contributions are relatively weak (Figure 4d), the structure introduced by modes 2–4 shifts peak semivariance to shorter lags (e.g., Figures 3a, 3c, and 3e). Semivariograms in these areas tend to rise steeply to maximum values at ~20–45 days and then drop somewhat over longer lags. A similar though weaker tendency is evident along the inner boundary of the SCB (e.g., Figure 3f) and along northernmost Baja.

4. Discussion

[33] We use EOF analysis of semivariograms to quantify and map patterns of intraseasonal variability across the CCS. Here we explore the possible origins of these patterns by demonstrating their association with patterns of physical and biological variability described by others. EOF analysis provides a concise description of coherent and widespread patterns of variability apparent in satellite-derived semivariograms, but may relegate locally meaningful structure to statistically insignificant higher modes. We investigate this possibility by comparing semivariograms calculated from co-located and concurrent time series of buoy and satellite-derived SST. We close this section with a discussion of the sampling characteristics of satellite-derived time series, and the possible effects of systematic sampling fluctuations on semivariogram structure.

4.1. Dominant Patterns of Intraseasonal Variability

[34] Mode 1 spatial amplitude functions (Figures 4c and 4d), particularly that of SST, resemble patterns of near-surface eddy kinetic energy (EKE) obtained by satellite altimetry. Elevated levels of inshore EKE reflecting energetic time-varying geostrophic currents lie within 100 km of the coast north of Cape Blanco but extend some 400–600 km offshore to the south and are surrounded by the low EKE of the open ocean [*Strub et al.*, 1997; *Strub and James*, 2000]. Wave number spectra calculated from multiyear time series of TOPEX cross-track velocity estimates show peak nearshore energy at wavelengths of ~300 km, a dominant wavelength associated with prominent meanders of the California Current core and the distances between neighboring eddies of the same rotational sense [*Kelly et al.*, 1998; *Strub and James*, 2000]. Similar calculations of frequency spectra from altimeter data are not available owing to aliased errors in modeled diurnal tides. However, *Strub et al.* [1997] qualitatively estimate dominant periods of 100–150 days for vector velocity estimates obtained from altimeter data at a point ~400 km offshore of northern California (37.1°N, 127.5°W). *Chereskin et al.* [2000] estimate dominant periods of 120–180 days from frequency spectra calculated from current meter data obtained at the same location, and *Kelly et al.* [1998] report peak energy at 120 days for currents measured at the base of the Ekman layer by an acoustic Doppler current profiler moored at that location. Dominant velocity fluctuations are forced by the movement of prominent eddies and meanders past fixed

locations [*Strub and James*, 2000], and their ~120 day periodicity corresponds to the dominant timescale of ~60 days revealed by the mode 1 EOFs of both SST and chlorophyll (Figures 4a and 4b). Note that mode 1 EOFs are not peaked and therefore provide no indication of regular, periodic variation. Although a third harmonic with a 120 day period could be included as a component of mean seasonality, semivariograms suggest that at these scales we should not assume SST and chlorophyll variability to be periodic. Nevertheless, mode 1 EOFs and spatial amplitude functions taken together suggest that the dominant structure of residual SST and chlorophyll time series is associated with the slow advection of mesoscale eddies and meanders.

[35] The elevated EKE of the CCS is a composite effect of the seasonal evolution of mesoscale circulation initiated with the springtime onset of strong and persistent upwelling winds and intensification of coastal currents [*Strub and James*, 2000]. The potential and kinetic energy of the upwelling front and jet are diverted into near-surface eddy energy through intrinsic instabilities, facilitated by coastal topography [*Marchesiello et al.*, 2003]. Dominant wavelengths of ~300 km presumably follow from the dominant contribution of EKE through baroclinic instability of coastal currents [*Strub and James*, 2000; *Marchesiello et al.*, 2003]. The seaward displacement and subsequent westward migration of the California Current core and associated EKE maxima is well documented by altimetry [*Kelly et al.*, 1998; *Strub and James*, 2000] and corroborated with multiyear, seasonally forced simulations [*Haney et al.*, 2001; *Marchesiello et al.*, 2003]. The simulated westward migration of EKE results from the westward propagation of individual eddies at speeds consistent with Rossby wave dynamics [*Marchesiello et al.*, 2003] and comparable to speeds of individual eddies observed off California and Baja [*Huyer et al.*, 1998; *Brink et al.*, 2000; *Soto-Mardones et al.*, 2004]. *Hormazabal et al.* [2004] offer a similar interpretation of near-surface velocity fluctuations within the Chilean upwelling system, suggesting that the slow westward migration of eddies and meanders generated near the coastline forces a dominant period of 120 days.

[36] Spatial patterns of intraseasonal SST and chlorophyll variance are consistent with dominant forcing through the distortion of large scale horizontal gradients by mesoscale jet and eddy activity. SST variance attributable to dominant structure (Figure 8a) is maximal off southern Oregon and southern Baja, areas of intense jet and eddy activity [e.g., *Barth et al.*, 2000; *Soto-Mardones et al.*, 2004] and also areas of strong seasonal SST gradients [*Legaard and Thomas*, 2006], where mesoscale circulation may be expected to induce the greatest variability. Spatial patterns of chlorophyll variance attributable to mode 1 structure are very similar to patterns of mean concentrations and nearshore annual and semiannual amplitudes [*Legaard and Thomas*, 2006], indicating a close coupling between the magnitude of dominant intraseasonal variability and the strength of seasonal surface gradients.

[37] Mode 1 SST and chlorophyll amplitude estimates (Figures 4c and 4d) are greatest where semivariogram shape adheres to that of the mode 1 EOF and where semivariogram structure is most clearly defined. Whereas measured and modeled near-surface EKE peaks off northern or central California [*Strub and James*, 2000; *Marchesiello et al.*, 2003], mode 1 amplitude estimates for both SST and chlorophyll tend to be greatest off southern California and Baja, in part because improved data availability [*Legaard and Thomas*, 2006] tends to reduce scatter between semivariance estimates (e.g., Figures 3f and 3h). Far offshore where resolved intraseasonal variance is weak, semivariogram shape is less clearly defined, scatter caused by cloud cover is more prominent, and amplitude estimates are low. Off north-central California, the outer boundary of elevated mode 1 amplitudes at ~128°W coincides with a drop in EKE which *Haney et al.* [2001] suggest is caused by the tendency for baroclinically unstable currents to become more barotropic in time, leading to a downward flux of EKE to the ocean interior. Across the northern CCS, the offshore drop in SST mode 1 amplitude coincides with a shift of peak semivariance to shorter timescales, as indicated by the greater influence of mode 2 (Figures 5c and 9a). This is not the case for chlorophyll, which shows a consistent shift toward shorter timescales only within ~100 km of the California coast. Across the southern CCS, the outer boundary of elevated mode 1 amplitude and EKE does not coincide with any coherent change in SST or chlorophyll semivariogram structure. Although *Strub and James* [2000] suggest a region-wide transition to shorter eddy spatial scales between 400 and 600 km from shore, such a transition is not reflected in or resolved by SST and chlorophyll semivariograms.

4.2. Deviations From Dominant Patterns of Intraseasonal Variability

[38] Variance introduced by modes 2–4 is generally small compared to variance contributed by the dominant mode 1 structure (compare Figures 8a–8b and 9a–9b). Between Cape Blanco and Cape Mendocino, the high-mode contribution for SST reflects a clear shift in peak semivariance to lags near 40 days (e.g., Figure 3a) suggesting some degree of periodicity at periods of ~80 days. It is not clear, however, whether peaked semivariograms reflect quasiperiodic SST fluctuations or dominance of a few episodic events of the appropriate 40-day duration. Here we can conclude only that a coherent and widespread shift toward timescales of ~40 days occurs across the northern CCS. Similarly, the high-mode contribution for chlorophyll reflects a shift in peak semivariance toward scales of ~20–45 days at inshore locations where mode 1 contributions are weak. North of Cape Mendocino, chlorophyll and SST semivariograms appear to peak at similar scales (e.g., Figure 3a). South of Cape Mendocino, chlorophyll semivariograms rise more rapidly to peak values at shorter time lags (e.g., Figures 3c, 3e, and 3f), indicating a greater amount of variability occurring over shorter timescales than for SST.

[39] Cape Mendocino tends to act as a climatological boundary between the sustained influence of the North Pacific high to the south and the frequent passage of storm systems to the north [*Dorman and Winant*, 1995]. Even during summer months when high pressure often extends into the Pacific Northwest, temporal patterns of wind-forcing have been observed to differ to the north and south of Cape Mendocino or Point Arena [*Kelly*, 1985; *Halliwell and Allen*, 1987; *Abbott and Barksdale*, 1991; *Largier et al.*, 1993], as have patterns of SST [*Kelly*, 1985]. It appears that

northern California lies at a transition in SST forcing between the dominant eddy variability to the south and the vigorous atmospheric forcing of higher latitudes, where strong Ekman drift or surface heat exchange may obscure the surface signature of propagating features originating at the coast [*Leeuwenburgh and Stammer*, 2001].

[40] *Denman and Abbott* [1994] found no significant difference between pattern decorrelation scales calculated from satellite SST and surface pigment concentrations off northern California. Their results suggest that over timescales of ~1–10 days and space scales of 25–100 km, phytoplankton act as passive tracers of mesoscale flow. The simultaneous response of SST and chlorophyll to mesoscale circulation and wind-forcing over timescales of several days is not necessarily inconsistent with divergent patterns of SST and chlorophyll variation over longer timescales of several weeks or more. However, meaningful comparisons between our results and those of *Denman and Abbott* [1994] are complicated by differences in methodology. Their analysis was based on select cloud-free late spring or early summer imagery, likely biased toward the high-wind, strong-upwelling conditions typically associated with clear skies [*Kelly*, 1985]. Our analysis integrates conditions from all seasons and a wider range of wind conditions. Their results are specific to SST and chlorophyll patterns of relatively small spatial scales (O(10–100 km)), whereas temporal structure estimated from empirical semivariograms includes variability acting over much larger spatial scales.

[41] Divergent patterns of SST and chlorophyll variability along the California Coast south of Cape Mendocino indicate that over timescales of several weeks to several months, SST may not act as a reliable indicator of the physical processes that drive variations in phytoplankton abundance. With increased distance/time from upwelling centers, SST is increasingly influenced by solar heating and is a less effective tracer of dynamics potentially important to phytoplankton patterns. The dominant phytoplankton of coastal upwelling regimes have evolved physiological traits and life history strategies that enable them to exploit the patterns of environmental variability characteristic of these regions [*Hutchings et al.*, 1995]. Variations in upwelling dynamics or associated patterns of mesoscale circulation may force divergent patterns of SST and chlorophyll variability by affecting specific aspects of phytoplankton ecology. For example, *Chavez et al.* [1991] and *Huyer et al.* [1991] describe the California Current core as it meandered seaward of Point Arena during the summer of 1988. The path of the current core remained stable for close to a month before rapidly realigning to a more alongshore orientation. Patterns of dynamic topography, surface temperature, and surface nitrate concentrations evolved in parallel throughout the survey sequence, but chlorophyll concentrations decreased dramatically in areas where nutrients remained high or actually increased. *Chavez et al.* [1991] suggest that the current realignment disrupted optimal conditions for diatom blooms, including perhaps seeding from upwelling source water. Such major current realignments may dominate chlorophyll distributions over timescales of several weeks or longer and may force the inshore shift in chlorophyll variance toward time lags of ~20–45 days. This shift is most clearly divergent from patterns of SST variation along the California coast south of Cape Mendocino.

4.3. Comparisons to In Situ Data

[42] *Largier et al.* [1993] describe an energetic band of current and surface temperature fluctuations over the northern California shelf and slope with periods longer than those of dominant wind-forcing. These fluctuations were attributed to mesoscale eddy variability in adjacent oceanic waters. Flow associated with impinging eddies was occasionally observed to dominate the local upwelling circulation for more than a month as warmer oceanic water flooded the inner shelf [*Largier et al.*, 1993]. Alternatively, the seaward displacement of eddies and meanders can provoke a realignment or reversal of local inshore currents, altering inshore SST patterns [*Huyer et al.*, 1991; *Lagerloef*, 1992]. Eddy-induced current fluctuations over the shelf and slope are typically dominated by periods on the order of 10–50 days, corresponding to decorrelation scales of 5–25 days [*Denman and Freeland*, 1985; *Largier et al.*, 1993; *Hickey*, 1998; *Chereskin et al.*, 2000]. *Breaker and Lewis* [1988] identified dominant 40–50 day periodic fluctuations in multiyear time series of in situ SST collected off central California. Fluctuations were coherent with alongshore winds at a phase lag consistent with forcing of SST by coastal upwelling, although *Breaker et al.* [2001] later showed that intraseasonal SST variability at this location was not always related to wind-forcing. *Dorman and Winant* [1995] found significant coherence between SST and alongshore winds over an energetic band of 5–50 day periods in buoy data collected along the U.S. West Coast. Phase lags were consistent with wind-forcing. We note features in individual empirical semivariograms at short scales (small sills, or breaks in slope) perhaps consistent with forcing at these shorter timescales. These features, however, are not consistently resolved in semivariograms of satellite-derived data and are not captured by EOFs. Both are dominated by greater variance at longer lags.

[43] We have calculated semivariograms from time series of in situ SST at several NOAA National Data Buoy Center (NDBC) stations. Long gaps are present at most stations. Here we select two relatively complete time series (locations shown in Figure 1), allowing direct comparisons between satellite-derived and in situ SST time series. Hourly buoy data were sampled at 1400 h, the nominal acquisition time of the AVHRR data used to construct Pathfinder SST time series. As with satellite data, seasonal and interannual variability were removed from buoy time series prior to the calculation of semivariograms. We then sampled collocated Pathfinder time series according to buoy data availability to produce the most sensible buoy-satellite data comparisons. Comparisons of empirical semivariograms from buoy and satellite time series (Figures 10a and 10b) show little difference in nugget effect and only slight differences in sill, but stronger scatter in satellite-measured semivariance. Buoy semivariance off Point Conception (NDBC station 46023, Figure 10b) increases more rapidly over time lags of ~5–20 days, suggesting greater SST variability at shorter timescales as might be expected in a point measurement compared to the 18 km spatial average of the satellite data. However, such a shift is not apparent off Point Arena (NDBC station 46014, Figure 10a). Consistent differences in semivariogram structure between the area-averaged Pathfinder data and the point data of buoy SST are not apparent across buoy stations. Sampling buoy time

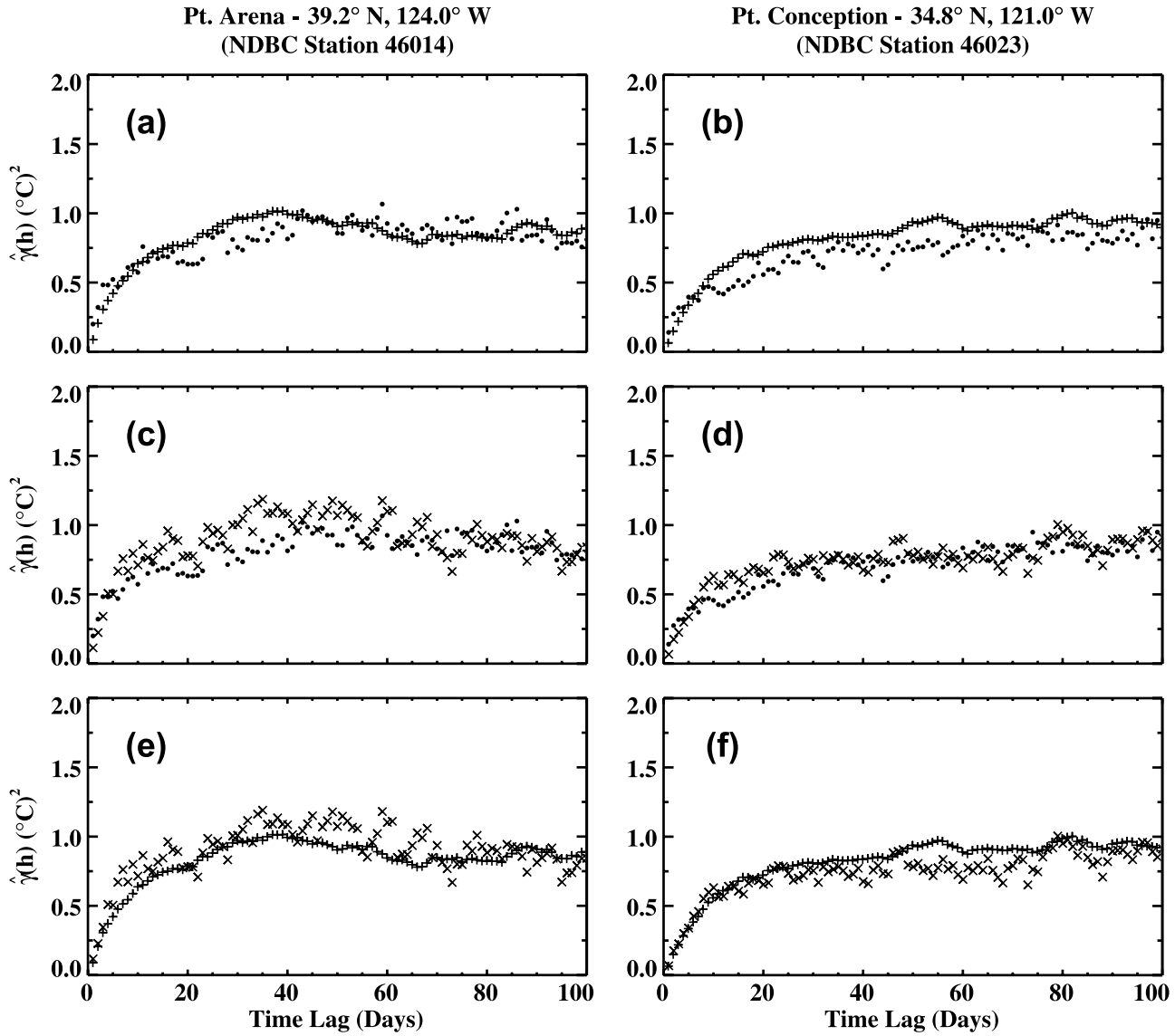

Figure 10. Empirical semivariograms calculated from Pathfinder SST and in situ SST time series collected at NDBC buoy stations off California (locations shown in Figure 1). (a–b) Semivariograms calculated from Pathfinder SST (●) and the full time series of buoy SST (+). (c-d) Semivariograms calculated from Pathfinder SST (●) and buoy SST sampled according to the availability of Pathfinder observations (×). (e-f) Semivariograms calculated from the full time series of buoy SST (+) and buoy SST sampled according to the availability of Pathfinder observations (×).

series according to valid satellite data retrievals (Figures 10c and 10d) increases the scatter of buoy semivariance to levels similar to the satellite data, indicating that missing data due to clouds is the primary contributor to scatter in satellite semivariograms.

[44] The way in which temporal sampling characteristics of satellite-derived time series may contribute to semivariogram structure was investigated using indicator semivariograms, defined as

$$\hat{\gamma}_I(h) = \frac{1}{2n(h)} \sum_{n(h)} [ind(t_i) - ind(t_i + h)]^2 \qquad (6)$$

where each indicator datum $ind(t_i)$ is set to 1 if an observation is available at time t_i and 0 if not. Indicator semivariance for a given time lag h is a measure of the frequency with which observations co-occur on days separated by that lag. A smaller value for a given lag implies a tendency for observations to co-occur on days separated by that time lag; a larger value implies a lesser tendency for observations to co-occur on days separated by that lag. The indicator semivariogram calculated from the Pathfinder SST time series from the upper slope of southern Baja (the empirical semivariogram of Figure 3h) oscillates with a period of 8–10 days (Figure 11), suggesting a tendency for observations to be systematically grouped at this sampling interval. Indicator semivariograms calculated from Pathfinder time series across much of the region possess the same periodic sampling structure, varying in strength with latitude and overall data availability, strongest

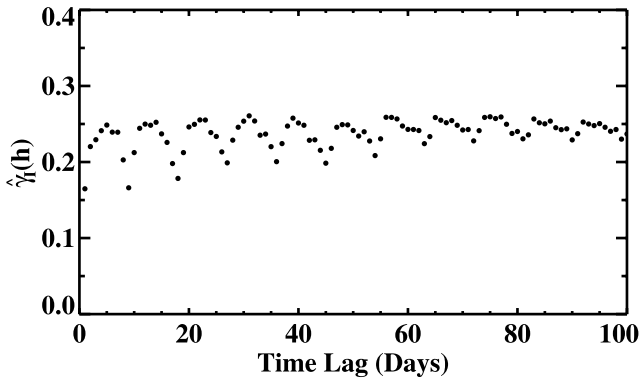

Figure 11. Indicator semivariogram calculated from the Pathfinder SST time series assembled at 26.0°N, 112.5°W (location shown in Figure 1).

off Punta Eugenia but virtually absent in the northern CCS. *Walker and Wilkin* [1998] identify a similar sampling structure in Pathfinder data over the Indo-Australian region and attribute its presence to satellite orbital dynamics and the width of the AVHRR instrument's field of view. They too note a latitudinal dependence, with sampling fluctuations strongest at lower latitudes. If sampling fluctuations are caused by orbital dynamics and sensor characteristics, then at any given latitude these fluctuations should be most apparent where time series are most complete and cloud cover the least persistent, as is the case off southern Baja.

[45] Across much of the southern CCS, 8–10 day sampling fluctuations appear to introduce 8–10 day fluctuations in empirical SST semivariograms (e.g., Figure 3h). These fluctuations are sufficiently strong and prevalent to have been captured by the mode 1 EOF (Figure 4a). Similar features are less apparent in semivariograms calculated from SeaWiFS chlorophyll. The potential influence of sampling structure on the calculation of SST semivariance is apparent when comparing complete buoy time series with buoy series sampled according to the days for which Pathfinder observations are available (Figures 10e and 10f). Although weaker at buoy stations than off Baja, sampling structure is capable of affecting the shape of empirical buoy semivariograms at short lags. Off Point Arena and Point Conception, semivariograms calculated from sampled buoy time series show a somewhat sharper break in slope at 8–10 days compared to semivariograms calculated from the full buoy time series (Figures 10e and 10f). Differences between buoy stations show that the impact, however, is variable and typically slight. The overall shapes of sampled buoy semivariograms retain the basic structure of semivariograms calculated from complete time series; nugget and sill values appear little affected. Although non-random patterns of data availability may affect relatively subtle features of satellite-derived semivariograms, we expect EOF analysis to reliably define widespread patterns apparent in the semivariance data.

5. Conclusions

[46] Here we use concurrent six year time series of daily satellite-derived SST and chlorophyll to quantify, map, and compare dominant patterns of intraseasonal variability from an EOF analysis of empirical semivariograms calculated across the CCS. Mode 1 EOFs for both chlorophyll and SST semivariograms indicate a dominant timescale of ~60 days. Spatial amplitudes and patterns of variance derived from mode 1 are consistent with dominant forcing of intraseasonal variability through distortion of large scale chlorophyll and SST gradients by mesoscale circulation. Intraseasonal SST variance is greatest off southern Baja and along southern Oregon and northern California. Chlorophyll variance is greatest over the shelf and slope, with elevated values closely confined to the Baja shelf and extending farthest from shore off California and the Pacific Northwest. As a fraction of total variance, intraseasonal SST variability is strongest near upwelling centers off southern Oregon and northern California where seasonal cycles are weakest. Intraseasonal variability accounts for the majority of total chlorophyll variance in most inshore areas save for southern Baja, where seasonal cycles dominate. Contributions of higher EOF modes to semivariogram structure reveal coherent deviations from dominant patterns of intraseasonal variability. SST variability shows a coherent shift toward timescales of ~40 days across much of the northern CCS. Dominant chlorophyll variability is consistently shifted to timescales of 20–45 days inshore. Scales of SST and chlorophyll variability diverge most markedly along the California coast between Point Conception and Cape Mendocino.

[47] Semivariograms provide a measure of average intraseasonal variance structure aggregated over the length of the data record. If patterns and overall levels of variability change in time, the shape of the semivariogram may preferentially reflect structure present during periods of high variance. Within the CCS, the mesoscale circulation that appears to force dominant intraseasonal variability of SST and chlorophyll is itself seasonally variable, sensitive to interannual events, and superimposed over seasonal and interannual variations in the intensity of large-scale gradients that in turn affect the magnitude of intraseasonal variance. The degree to which specific scales of variability are reflected in the shapes of SST and chlorophyll semivariograms will thereby depend, in part, on the relative timing of evolving mesoscale and large-scale patterns.

[48] We acknowledge cautious interpretation of fundamentally nonstationary data as if they were stationary. Intraseasonal variation is characteristically intermittent and episodic in nature and our quantification includes contributions from interannual anomalies resulting from phase shifts in seasonal cycles. These contributions, however, are an important aspect of both SST and chlorophyll variability in the CCS. The strength of semivariograms lies in their ability to reliably identify dominant scales in geophysical data. Their weakness is an inability to reliably resolve multiple scales within nonstationary data. Semivariograms and related methods provide a parsimonious description of patterns of variability over large regions but require complementary approaches, such as state-space analysis [e.g., *Schwing and Mendelssohn*, 1997] and wavelet analysis [e.g., *Breaker et al.*, 2001; *Henson and Thomas*, 2007], to resolve nonstationary signals and changes in the dominance of specific scales of variation through time/space. However, all approaches using infrared and visible satellite data will meet limitations imposed by gaps due to cloud cover at the

shortest timescales. Patterns of intraseasonal variability quantified here and patterns of mean seasonality and interannual variability presented by *Legaard and Thomas* [2006] summarize the spatial dependence of dominant scales of SST and chlorophyll variability across the CCS.

[49] **Acknowledgments.** We gratefully acknowledge the efforts of the NASA SeaWiFS Science Project and the GSFC DAAC for their efforts in making the SeaWiFS data available, the NOAA/NASA AVHRR Oceans Pathfinder project and the JPL PODAAC for access to the Pathfinder SST data, and the NOAA NDBC for access to buoy data. We thank Phaedon Kyriakidis for suggesting EOF analysis to describe semivariogram data sets. Support for this project was provided by NSF grants 0000899, 0531289 and 0535386 to ACT. Contribution number 544 from the U.S. GLOBEC Program.

References

Abbott, M. R., and B. Barksdale (1991), Phytoplankton pigment patterns and wind forcing off central California, *J. Geophys. Res.*, *96*, 14,649–14,667.

Armstrong, E. M. (2000), Satellite derived sea surface temperature variability off California during the upwelling season, *Remote Sens. Environ.*, *73*, 1–17.

Barth, J. A., S. D. Pierce, and R. L. Smith (2000), A separating coastal upwelling jet at Cape Blanco, Oregon and its connection to the California Current System, *Deep Sea Res. II*, *47*, 783–810.

Breaker, L. C., and P. A. W. Lewis (1988), A 40–50 day oscillation in sea-surface temperature along the central California coast, *Est. Coast. Shelf Sci.*, *26*, 395–408.

Breaker, L. C., P. C. Liu, and C. Torrence (2001), Intraseasonal oscillations in sea surface temperature, wind stress, and sea level off the central California coast, *Cont. Shelf Res.*, *21*, 727–750.

Brink, K. H., R. C. Beardsley, J. Paduan, R. Limeburner, M. Caruso, and J. G. Sires (2000), A view of the 1993–1994 California Current based on surface drifters, floats, and remotely sensed data, *J. Geophys. Res.*, *105*, 8575–8604.

Campbell, J. W. (1995), The lognormal distribution as a model for bio-optical variability in the sea, *J. Geophys. Res.*, *100*, 13,237–13,254.

Chavez, F. P., R. T. Barber, P. M. Kosro, A. Huyer, S. R. Ramp, T. P. Stanton, and B. R. de Mendiola (1991), Horizontal transport and distribution of nutrients in the coastal transition zone off northern California: Effects on primary production, phytoplankton biomass and species composition, *J. Geophys. Res.*, *96*, 14,833–14,848.

Chereskin, T. K., M. Y. Morris, P. P. Niiler, P. M. Kosro, R. L. Smith, S. R. Ramp, C. A. Collins, and D. L. Musgrave (2000), Spatial and temporal characteristics of the mesoscale circulation of the California Current from eddy-resolving moored and shipboard measurements, *J. Geophys. Res.*, *105*, 1245–1269.

Cressie, N., and D. M. Hawkins (1980), Robust estimation of the variogram, *J. Int. Assoc. Math. Geol.*, *12*, 115–125.

Denman, K. L., and M. R. Abbott (1988), Time evolution of surface chlorophyll patterns from cross-spectrum analysis of satellite color images, *J. Geophys. Res.*, *93*, 6789–6798.

Denman, K. L., and M. R. Abbott (1994), Time scales of pattern evolution from cross-spectrum analysis of advanced very high resolution radiometer and coastal zone color scanner imagery, *J. Geophys. Res.*, *99*, 7433–7442.

Denman, K. L., and H. J. Freeland (1985), Correlation scales, objective mapping and a statistical test of geostrophy over the continental shelf, *J. Mar. Res.*, *43*, 517–539.

Doney, S. C., D. M. Glover, S. J. McCue, and M. Fuentes (2003), Mesoscale variability of SeaWiFS satellite ocean color: Global patterns and spatial scales, *J. Geophys. Res.*, *108*(C2), 3024, doi:10.1029/2001JC000843.

Dorman, C. E., and C. D. Winant (1995), Buoy observations of the atmosphere along the west coast of the United States, 1981–1990, *J. Geophys. Res.*, *100*, 16,029–16,044.

Fuentes, M., S. C. Doney, D. M. Glover, and S. J. McCue (2001), Spatial structure of the SeaWiFS ocean color data for the North Atlantic Ocean, in *Studies in the atmospheric sciences (Lecture notes in statistics Vol. 144)*, edited by M. Berliner, D. Nychka, and T. Hoar, pp. 153–171, Springer-Verlag, New York.

Gallaudet, T. C., and J. J. Simpson (1994), An empirical orthogonal function analysis of remotely sensed sea surface temperature variability and its relation to interior oceanic processes off Baja California, *Remote Sens. Environ.*, *47*, 375–389.

Goovaerts, P. (1997), *Geostatistics for natural resources evaluation*, Oxford Univ. Press, New York.

Halliwell, G. R., and J. S. Allen (1987), The large-scale coastal wind field along the west coast of North America, 1981–1982, *J. Geophys. Res.*, *92*, 1861–1884.

Haney, R. L., R. A. Hale, and D. E. Dietrich (2001), Offshore propagation of eddy kinetic energy in the California Current, *J. Geophys. Res.*, *106*, 11,709–11,717.

Henson, S. A., and A. C. Thomas (2007), Phytoplankton scales of variability in the California Current system: 1. Interannual and cross-shelf variability, *J. Geophys. Res.*, *112*, C07017, doi:10.1029/2006JC004039.

Hickey, B. M. (1998), Coastal oceanography of western North America from the tip of Baja California to Vancouver Island, in *The Sea*, Vol. 11, edited by A. R. Robinson and K. H. Brink, pp. 345–393, John Wiley, New York.

Hormazabal, S., G. Shaffer, and O. Leth (2004), Coastal transition zone off Chile, *J. Geophys. Res.*, *109*, C01021, doi:10.1029/2003JC001956.

Hutchings, L., G. C. Pitcher, T. A. Probyn, and G. W. Bailey (1995), The chemical and biological consequences of coastal upwelling, in *Upwelling in the ocean: Modern processes and ancient records*, edited by C. P. Summerhayes, K.-C. Emeis, M. V. Angel, R. V. Smith, and B. Zeitzschel, pp. 65–81, John Wiley, New York.

Huyer, A., P. M. Kosro, J. Fleischbein, S. R. Ramp, T. Stanton, L. Washburn, F. P. Chavez, T. J. Cowles, S. D. Pierce, and R. L. Smith (1991), Currents and water masses of the coastal transition zone off northern California, June to August 1988, *J. Geophys. Res.*, *96*, 14,809–14,831.

Huyer, A., J. A. Barth, P. M. Kosro, R. K. Shearman, and R. L. Smith (1998), Upper-ocean water mass characteristics of the California current, Summer 1993, *Deep Sea Res. II*, *45*, 1411–1442.

Kelly, K. A. (1985), The influence of winds and topography on the sea surface temperature patterns over the northern California slope, *J. Geophys. Res.*, *90*, 11,783–11,789.

Kelly, K. A., R. C. Beardsley, R. Limeburner, K. H. Brink, J. D. Paduan, and T. K. Chereskin (1998), Variability of the near-surface eddy kinetic energy in the California Current based on altimetric, drifter, and moored current data, *J. Geophys. Res.*, *103*, 13,067–13,083.

Kilpatrick, K. A., G. P. Podestá, and R. Evans (2001), Overview of the NOAA/NASA Pathfinder algorithm for sea surface temperature and associated match-up database, *J. Geophys. Res.*, *106*, 9179–9198.

Lagerloef, G. S. E. (1992), The Point Arena eddy: A recurring summer anticyclone in the California Current, *J. Geophys. Res.*, *97*, 12,557–12,568.

Largier, J. L., B. A. Magnell, and C. D. Winant (1993), Subtidal circulation over the northern California shelf, *J. Geophys. Res.*, *98*, 18,147–18,179.

Leeuwenburgh, O., and D. Stammer (2001), The effect of ocean currents on sea surface temperature anomalies, *J. Phys. Oceanogr.*, *31*, 2340–2358.

Legaard, K. L., and A. C. Thomas (2006), Spatial patterns in seasonal and interannual variability of chlorophyll and sea surface temperature in the California Current, *J. Geophys. Res.*, *111*, C06032, doi:10.1029/2005JC003282.

Lewis, M. R., N. Kuring, and C. Yentsch (1988), Global patterns of ocean transparency: Implications for the new production of the open ocean, *J. Geophys. Res.*, *93*, 6847–6856.

Lynn, R. J., and J. J. Simpson (1987), The California Current System: The seasonal variability of its physical characteristics, *J. Geophys. Res.*, *92*, 12,947–12,966.

Mackas, D. L., P. T. Strub, A. C. Thomas, and V. Montecino (2006), Eastern ocean boundaries pan-regional view, in *The Sea*, Vol. 14, edited by A. R. Robinson and K. H. Brink, pp. 21–60, Harvard Univ. Press, Cambridge, Mass.

Marchesiello, P., J. C. McWilliams, and A. Shchepetkin (2003), Equilibrium structure and dynamics of the California Current System, *J. Phys. Oceanogr.*, *33*, 753–783.

Nelson, C. S., and D. M. Husby (1983), Climatology of surface heat fluxes over the California current region, *NOAA Tech. Rep. NMFS SSRF-763*, U.S. Dept. of Commerce, Washington, D.C.

O'Reilly, J. E., et al. (2000), Ocean color chlorophyll *a* algorithms for SeaWiFS, OC2, and OC4: Version 4, in *SeaWiFS Postlaunch Calibration and Validation Analyses*, Part 3, edited by S. B. Hooker and E. R. Firestone, *NASA Tech. Memo. 206892*, Vol. 11, 9-23, NASA Goddard Space Flight Center, Greenbelt, Maryland.

Overland, J. E., and R. W. Preisendorfer (1982), A significance test for principal components applied to a cyclone climatology, *Mon. Weather Rev.*, *110*, 1–4.

Schwing, F. B., and R. Mendelssohn (1997), Increased coastal upwelling in the California Current System, *J. Geophys. Res.*, *102*, 3421–3438.

Smith, R. L. (1995), The physical processes of coastal ocean upwelling systems, in *Upwelling in the ocean: Modern processes and ancient records*, edited by C. P. Summerhayes, K.-C. Emeis, M. V. Angel, R. V. Smith, and B. Zeitzschel, pp. 39–64, John Wiley, New York.

Smith, R. C., X. Zhang, and J. Michaelsen (1988), Variability of pigment biomass in the California Current System as determined by

satellite imagery 1. Spatial variability, *J. Geophys. Res.*, *93*, 10,863–10,882.

Soto-Mardones, L., A. Parés-Sierra, J. Garcia, R. Durazo, and S. Hormazabal (2004), Analysis of the mesoscale structure in the IMECOCAL region (off Baja California) from hydrographic, ADCP and altimetry data, *Deep Sea Res. II*, *51*, 785–798.

Strub, P. T., and C. James (1988), Atmospheric conditions during the spring and fall transitions in the coastal ocean off western United States, *J. Geophys. Res.*, *93*, 15,561–15,584.

Strub, P. T., and C. James (2000), Altimeter-derived variability of surface velocities in the California Current System: 2. Seasonal circulation and eddy statistics, *Deep Sea Res. II*, *47*, 831–870.

Strub, P. T., J. S. Allen, A. Huyer, and R. L. Smith (1987), Large-scale structure of the spring transition in the coastal ocean off western North America, *J. Geophys. Res.*, *92*, 1527–1544.

Strub, P. T., C. James, A. C. Thomas, and M. R. Abbott (1990), Seasonal and nonseasonal variability of satellite-derived surface pigment concentration in the California Current, *J. Geophys. Res.*, *95*, 11,501–11,530.

Strub, P. T., P. M. Kosro, A. Huyer, and CTZ Collaborators (1991), The nature of cold filaments in the California Current system, *J. Geophys. Res.*, *96*, 14,743–14,768.

Strub, P. T., T. K. Chereskin, P. P. Niiler, C. James, and M. D. Levine (1997), Altimeter-derived variability of surface velocities in the California Current System: 1. Evaluation of TOPEX altimeter velocity resolution, *J. Geophys. Res.*, *102*, 12,727–12,748.

Thomas, A. C., and W. J. Emery (1988), Relationships between near-surface plankton concentrations, hydrography, and satellite-measured sea surface temperature, *J. Geophys. Res.*, *93*, 15,733–15,748.

Thomas, A., and P. T. Strub (2001), Cross-shelf phytoplankton pigment variability in the California Current, *Cont. Shelf Res.*, *21*, 1157–1190.

Thomas, A. C., M.-E. Carr, and P. T. Strub (2001), Chlorophyll variability in eastern boundary currents, *Geophys. Res. Lett.*, *28*, 3421–3424.

Uz, B. M., and J. A. Yoder (2004), High frequency and mesoscale variability in SeaWiFS chlorophyll imagery and its relation to other remotely sensed oceanographic variables, *Deep Sea Res. II*, *51*, 1001–1017.

Vazquez, J., K. Perry, and K. Kilpatrick (1998), NOAA/NASA AVHRR oceans pathfinder sea surface temperature data set user's reference manual, version 4.0, *Jet Propulsion Laboratory Pub., 74* (D-14070), Jet Propulsion Laboratory, Pasadena, California.

Walker, A. E., and J. L. Wilkin (1998), Optimal averaging of NOAA/NASA Pathfinder satellite sea surface temperature data, *J. Geophys. Res.*, *103*, 12,869–12,883.

Webster, R., and M. A. Oliver (2001), *Geostatistics for environmental scientists*, John Wiley, Chichester.

Yoder, J. A., C. R. McClain, J. O. Blanton, and L.-Y. Oey (1987), Spatial scales in CZCS-chlorophyll imagery of the southeastern U.S. continental shelf, *Limnol. Oceanogr.*, *32*, 929–941.

Yoder, J. A., J. E. O'Reilly, A. H. Barnard, T. S. Moore, and C. M. Ruhsam (2001), Variability in coastal zone color scanner (CZCS) chlorophyll imagery of ocean margin waters off the U.S. East Coast, *Cont. Shelf Res.*, *21*, 1191–1218.

K. R. Legaard and A. C. Thomas, School of Marine Sciences, University of Maine, Orono, ME 01169-5755, USA. (kasey_legaard@umit.maine.edu)